Historical masonry building aggregates: Advanced numerical insight for an effective seismic assessment on two row housing compounds

by
Marco VALENTE[(1)], Gabriele MILANI[*(1)], Ernesto GRANDE[(2)], Antonio FORMISANO[(3)]

(1) Department of Architecture, Built Environment and Construction Engineering Politecnico di Milano, Piazza Leonardo da Vinci 32, 20133 Milano, Italy
(2) Department of Sustainability Engineering, University Guglielmo Marconi, Via Plinio 44, 00193 Rome, Italy
(3) Dept. of Structures for Engineering and Architecture, University of Naples "Federico II", Naples, Italy
** Corresponding author. E-mail: gabriele.milani@polimi.it*
Phone: +39 022399 4290 Fax: +39 022399 4220

Abstract

Historical masonry aggregates represent a large portion of the cultural heritage in Italy and are highly vulnerable to seismic actions, as shown by past seismic events. Typically, they are large and complex structures for which there is a lack of knowledge and information concerning the structural behavior, in particular as far as the response to seismic actions is concerned. This paper investigates the seismic response of two complex historical masonry aggregates located in Sora (Lazio region, central Italy), through advanced 3D FE numerical simulations. For each aggregate, a detailed 3D FE model is developed and analyzed in the non-linear dynamic range, assuming that masonry behaves as a damaging-plastic material with almost vanishing tensile strength. The seismic performance of the two aggregates is evaluated in terms of damage distribution, energy density dissipated by tensile damage and maximum normalized displacements. The numerical analyses show the high vulnerability of the perimeter walls. In particular, the units at the extremities of the aggregate are subjected to large displacements, being not efficiently braced by the adjacent units and being subjected to the torsional effects induced by the seismic action. The presence of several openings is a fundamental feature that significantly decreases the strength of the perimeter walls, influencing the damage distribution in the aggregate mainly due to out-of-plane actions. The most damaged elements are generally the walls of the tall units without lateral support and the adjacent slabs covering large spans. Numerical results show that the structural response of a single building unit is affected by the interactions with adjacent structural parts. Moreover, it can be stated that a preliminary structural assessment through kinematic limit analysis on partial failure mechanisms may be reliable only after a proper estimation of the different structural elements playing a role in the horizontal behavior (e.g. interlocking between walls, typology of masonry, distribution of horizontal loads, constraints and dead loads distribution, etc.). The obtained results will be used in an accompanying paper to benchmark simplified approaches that can be used by engineers in common design practice to quickly predict the seismic vulnerability of the aggregates and define the most suitable strengthening interventions.

Keywords: masonry aggregate; seismic response; damage assessment; full 3D FE models; non-linear dynamic analysis

1. Introduction

Unreinforced masonry buildings represent a large portion of the building stock in several earthquake-prone countries, such as Italy [1][2]. The majority of these buildings are not isolated, but aggregated in clusters dating back to the Middle Age. They are widespread everywhere in Europe, but especially in Italian historical city centers [3]-[10].

More specifically, historical masonry aggregates are large and complex structures that generally consist of several adjacent structural units erected in continuity one to each other. They were conceived to resist only gravity loads without seismic design criteria and are often composed of structural units with different height, number of stories and inter-story height.

In agreement with intuition, from the above considerations it can be stated that the seismic vulnerability assessment of existing masonry aggregates in historical centers represents both an open issue and a very difficult task, mainly for two reasons: (1) lack of adequate numerical tools able to take into account the complexity of the problem (geometry, material non-linearity, presence of local strengthening, correct evaluation of the stiffness of floors and roofs, etc) in an efficient way; (2) little knowledge of crucial features (e.g. actual interlocking between perpendicular walls, real masonry texture along the thickness, presence of local strengthening devices, etc.). For such reasons, the vulnerability assessment of large masonry aggregates has not been investigated so much by the scientific community in the recent past and the information on their structural behavior, particularly as regards their seismic response, is still at its embryonic stage. It is not a coincidence, indeed, that the current Italian code [11]-[13] does not provide reliable methodologies and detailed procedures for the seismic assessment of such typology of structures.

In the literature, simplified methods have been proposed to perform speedy large scale [14][15] or more detailed local scale [16]-[18] seismic vulnerability evaluations, but the estimation of their actual reliability seems still missing, because it should be made using sophisticated full 3D FE non-linear dynamic computations. Pushover computations have been performed on full 3D complex models or equivalent frames with the aim of estimating the vulnerability of building aggregates in Baixa Pombalina quarter in Lisbon [19][20]. The application of a non-linear dynamic excitation appears however prohibitive in the first case or questionable in the second one, where the cyclic behavior of concentrated hinges is not easily deducible at a sectional level. The Distinct Element Method (DEM) [21]-[25] could be an interesting alternative, but whilst literature seems to be consolidated in micro-modelling, the utilization of macro-elements appears still very limited [26]. DEM has indeed the advantage that is conceptually simple (also in the implementation of contact and friction between blocks [27]) and allows effectively performing fast and reliable non-linear dynamic analyses. One of the main open problems is however the correct definition of both macro-elements and interface mechanical properties, which could be found using, for instance, the most updated limit analysis procedures with optimization/adaptation of the mesh combined with homogenization [28][29].

As a matter of fact, a seismic response assessment of such a typology of structures that can be adopted as reference certainly requires the analysis of the whole aggregate, taking into account all the structural units composing the aggregate together in a single step. Moreover, in some cases the definition and identification of a structural unit may result somewhat questionable and methods based on constraining a single unit with lateral springs at given equivalent stiffness are by definition debatable and for sure limited in the effectiveness to specific case-studies. In this complex framework, reliable numerical approaches and analysis methods may represent necessary tools to evaluate the structural behavior of masonry aggregates. In the literature, there are several significant examples of application of the non-linear finite element (FE) method to study the seismic response of historical masonry constructions, but mainly applied to isolated structures, such as churches, towers and palaces [30]-[35].

The present study is aimed at presenting a complex real example, whose results can be taken as reference to validate any simplified approach applicable to building aggregates in common practice. An important aspect is clearly pointed out in this work: advanced FE analyses should be regarded as

a preferential research procedure able to provide significant information on the seismic behavior of historical masonry aggregates. Such an approach is expected to be the closest one to reality and hence eligible to be considered as benchmark for all those alternative approaches based on successive simplifications that can be used in daily design.

An accompanying paper [36], following the present one, will show that a "reasoned" utilization of (1) kinematic limit analysis on partial failure mechanisms and (2) pushover analyses with equivalent frames conducted on both whole aggregate and single units, may lead to preliminary predictions of the seismic vulnerability not far from those provided by the present complex 3D FE non-linear dynamic computations.

The benchmark here discussed relies on the seismic performance evaluation of two existing traditional masonry building aggregates located in the city of Sora, Central Italy [37][38]. One of the most common typologies of masonry aggregates in Italian historical centers is the so called row housing typology, consisting of a series of structural units arranged in line along the longitudinal axis parallel to the street: it corresponds to the case here treated and indeed the two aggregates face the same street.

For each aggregate, a detailed three-dimensional finite element (FE) model is developed and analyzed in the non-linear dynamic range. It is assumed that masonry behaves as an isotropic material with damage and plasticization in both tension and compression, with different strength and damage parameters in tension and compression and cohesive frictional behavior under shear actions. The modelling technique adopted, therefore, is based on the so-called macro-modelling approach (units and mortar are smeared in a fictitious homogeneous material at a structural level), the only one possible for very large scale examples, but exhibiting at the macro-scale a behavior not far from that shown by a quasi no-tension material. In particular, the analyses are carried out considering the same material for all the units with properties derived from little information available. This assumption certainly affects the results obtained in terms of global seismic capacity and damage patterns. Nevertheless, as underlined in the following sections, it allows emphasizing aspects specifically related to the global behavior of masonry aggregates and the interaction among the units. It is evident that additional information concerning both the masonry material and structural details allow capturing further aspects of the response, such as failure modes related to structural deficiencies that are not included in the proposed model. Such additional information can represent a subsequent detailed step of analysis.

The seismic performance of the two aggregates is evaluated in terms of damage distribution, energy density dissipated by tensile damage and maximum normalized displacements. The numerical analyses show the high vulnerability of the perimeter walls that may be subjected to overturning mechanisms. In particular, the units at the extremities of the aggregate are subjected to large displacements, being not efficiently braced by the adjacent units and being subjected to the torsional effects induced by the seismic action. The presence of several openings is another crucial feature that significantly decreases the strength of the perimeter walls, influencing the damage distribution in the aggregate and out-of-plane partial collapses. It is important to observe that the most damaged elements turn out to be, generally, the walls of the tall units without lateral support and the adjacent slabs covering large spans. Numerical results show that the structural response of a single building unit is affected by the interactions with adjacent structural parts and that an assessment by means of the kinematic limit analysis on partial failure mechanisms may be reliable, but only after an adequate estimation of all those aspects playing a role in the horizontal behavior. In particular, the interlocking between walls, typology of masonry, distribution of horizontal loads, lateral constraints and vertical and horizontal loads distribution turn out to be paramount.

The paper is organized as follows. Section 2 describes the main characteristics of the two aggregates under study. Section 3 shows the FE model of the aggregates and the damage model adopted for masonry. The results of the advanced numerical simulations performed on both the aggregates are presented in Section 4. Section 5 compares and discusses the main results obtained from the numerical analyses. The main conclusions of the work are summarized in Section 6.

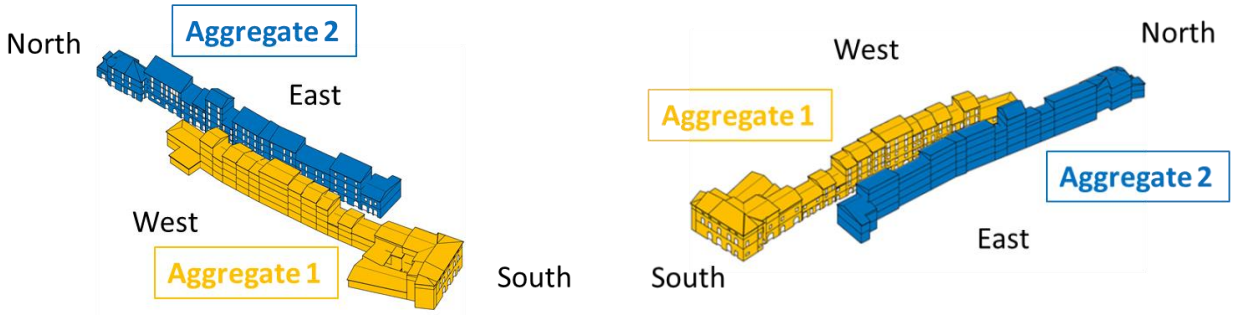

Figure 1. Two schematic views of the two aggregates under study: Aggregate 1 (yellow color) and Aggregate 2 (blue color).

2. Description of the aggregates under study

The compound of Borgo San Rocco is located in the municipality of Sora in Lazio region, Central Italy. It is composed of two aggregates facing each other and divided by Borgo San Rocco street. In this study, the west aggregate is named Aggregate 1 and the east aggregate is named Aggregate 2: two rough schematic views of the volumes and relative positions of the two aggregates are shown in Figure 1. The geometrical characteristics of the two aggregates approximately recall the features of the row housing typology, which is very widespread in Italian historical centers [37][38]. A very short description of the main features of the two aggregates under study is presented in the following.

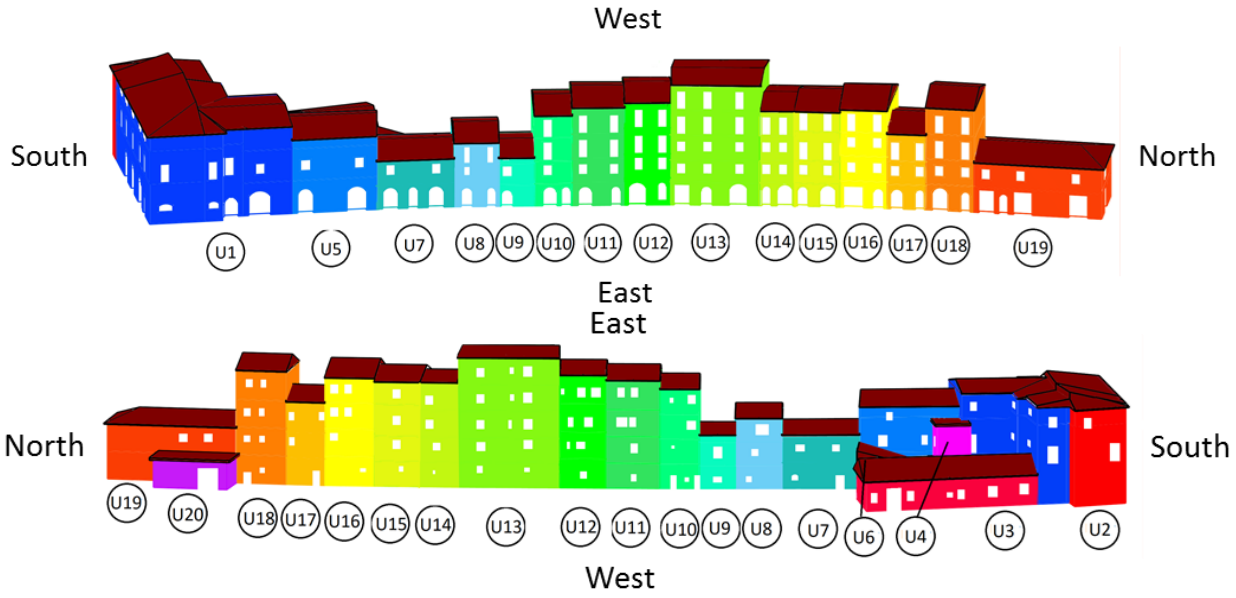

Figure 2. Aggregate 1: schematic drawings (plan, front view, section) and indication of the different structural units.

2.1.Aggregate 1

Aggregate 1, which is located on the west side of Borgo San Rocco street, is oriented longitudinally along the north-south direction; it is about 120 m long and consists of 20 structural units characterized by masonry load-bearing walls. The structural units composing the aggregate present different storeys and the height varies considerably along the construction: the smallest units are composed of a single storey, while the highest units present up to four stories. The maximum height is 15.4 m in correspondence with unit U13, while the smallest unit U20 on the back (west) side of the aggregate is 3.35 m high.

The transversal dimension (width) of Aggregate 1 is variable and maximum (about 24 m) at the southern extremity, in correspondence with units U1 and U2. In the central-northern part, which is characterized by single-room structural units, the width is quite uniform and equal to about 7.5 m, while at the northern extremity, in correspondence with units U19 and U20, it is equal to about 13 m. The external walls exhibit a quite uniform thickness (60-70 cm), while the thickness of the internal walls varies between 30 and 70 cm.

A large variety of coverings typologies can be found: masonry barrel vaults (mainly at the ground floor), concrete-masonry slabs, wooden slabs, flooring blocks and steel beams. Several openings are present on each side of the aggregate, especially on the front (east) side; they are particularly numerous in the central part, while at the two extremities their number is smaller. On the back (west) side, there are several windows and very few doors.

Figure 2 shows the schematic drawings of Aggregate 1 along with some geometrical dimensions and an indication of the different structural units.

2.2. Aggregate 2

Aggregate 2, which is located on the east side of Borgo San Rocco street, is oriented longitudinally along the north-south direction; it is about 120 m long and consists of 12 structural units characterized by masonry load-bearing walls.

The structural units composing the aggregate present different storeys and height. The lowest units consist of two storeys, while the highest one exhibits up to five storeys. In detail, the maximum height is about 16 m in correspondence with unit U5 in the central part, while the smallest unit U1 located in the northern part is about 6.1 m high.

The transversal dimension (width) of Aggregate 2 is more uniform than that of Aggregate 1, reaching the maximum value in the southern extremity (unit U12): the width is about 13 m in correspondence with unit U12, while it is more uniform and about 6 m in the remaining part of the aggregate.
The thickness of the external walls is quite uniform (about 60 cm), with some exceptions, such as the northern wall of unit U1 that is 50 cm thick. The thickness of the internal walls varies between 30 and 65 cm.
A large variety of coverings typologies can be found: masonry barrel vaults, concrete-masonry slabs, wooden slabs, flooring blocks and steel beams. The coverings of the ground floor and in the south part generally consist of barrel vaults. On the front (west) side of the aggregate there are several openings (windows and doors), while the back (east) side presents very few openings (only small windows).
Figure 3 shows the schematic drawings of Aggregate 2 along with some geometrical dimensions and an indication of the different structural units.

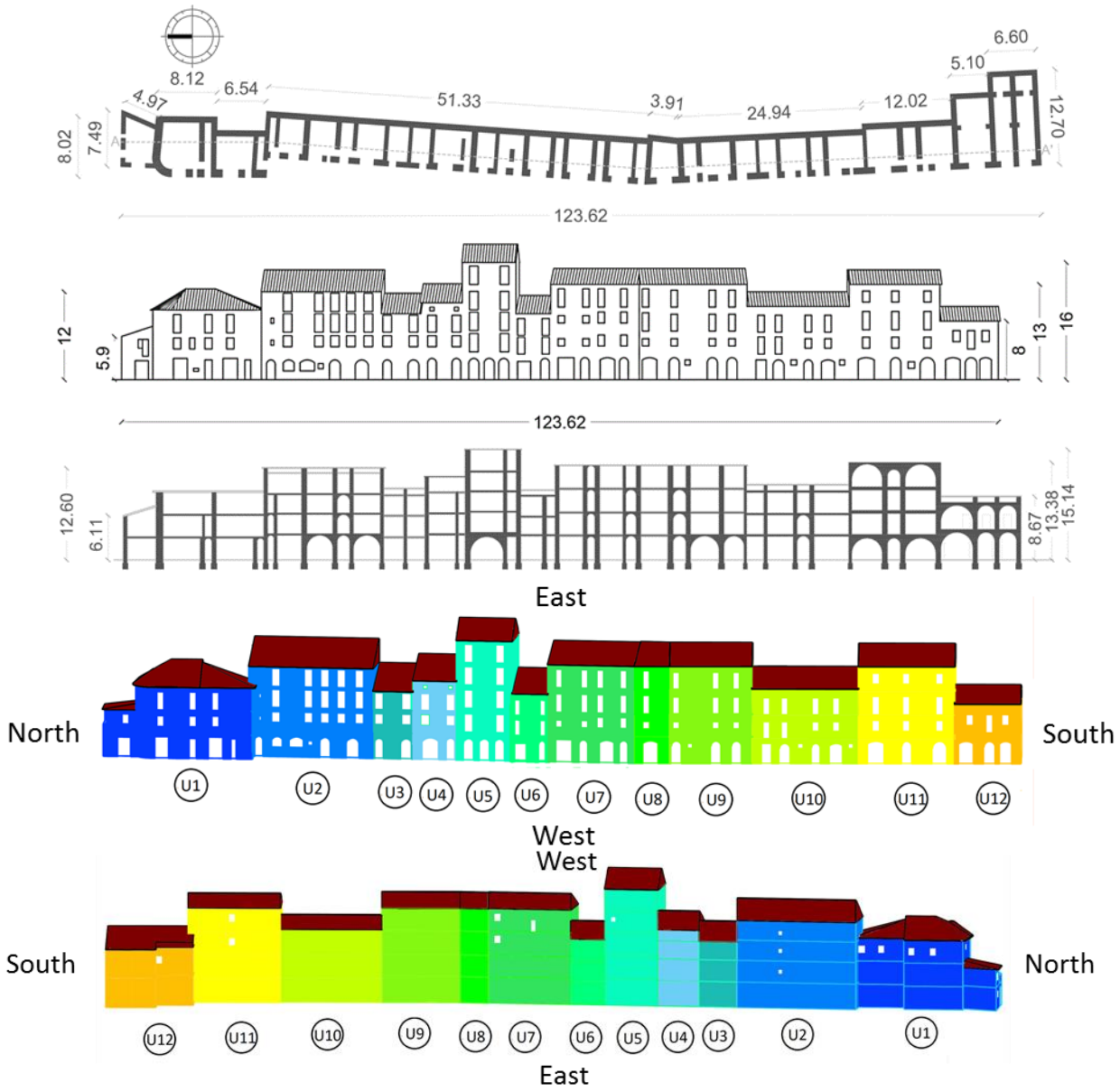

Figure 3. Aggregate 2: schematic drawings (plan, front view, section) and indication of the different structural units.

3. FE models and material model adopted

Detailed three-dimensional FE models of the two aggregates under study are developed through the computer code Abaqus using four-node tetrahedral solid elements [39]. The complex geometry of the aggregates is reproduced accurately using the drawings and the data collected from existing available documentations. Figure 4 and Figure 5 show different views of the geometrical and FE models of Aggregate 1 and Aggregate 2, respectively. The numerical models are created considering the load-bearing masonry walls, masonry vaults and the concrete-masonry slabs present in the aggregate as floors coming from recent interventions. Arches and vaults have been considered in the numerical simulations, modeling also the infill, where present, through few 3D elements with poor mechanical properties.

As it generally occurs in historical structures, the most diffused typology of floors in the aggregate system is constituted by traditional wooden slabs supported by wooden beams simply supported by perimeter masonry walls. In some few cases, a system with steel beams with small tile vaults has

been used. In both cases, their stiffness is typically considered negligible, hence they are not reported in the FE model. Gravity loads are therefore directly transferred to masonry piers as distributed pressures. Analogously, wooden and steel beams are not represented in the FE mesh, implicitly renouncing to account for the possible punching of beam head on the walls induced by the earthquake. Such a typology of collapse is certainly important, but very local and characterized by masonry crumbling, especially if masonry is constituted by mortar with very poor mechanical properties and blocks are stiff and relatively resistant. Crumbling is a phenomenon hardily reproducible with continuous damaging models, as that used in this study, which requires the utilization of DEM [23][27]. Finally, the mesh refinement utilized, as a consequence of the considerable dimensions of the aggregate, is unavoidably not suited to accurately reproduce such a type of local phenomenon. Moreover, it is worth mentioning that some approximations of the geometrical features of the two aggregates are introduced in some cases, because of the inherent complexity of the structures under study: despite such modifications, the FE models provide two representative case studies useful to have an insight into the seismic performance assessment of such typologies of structures.

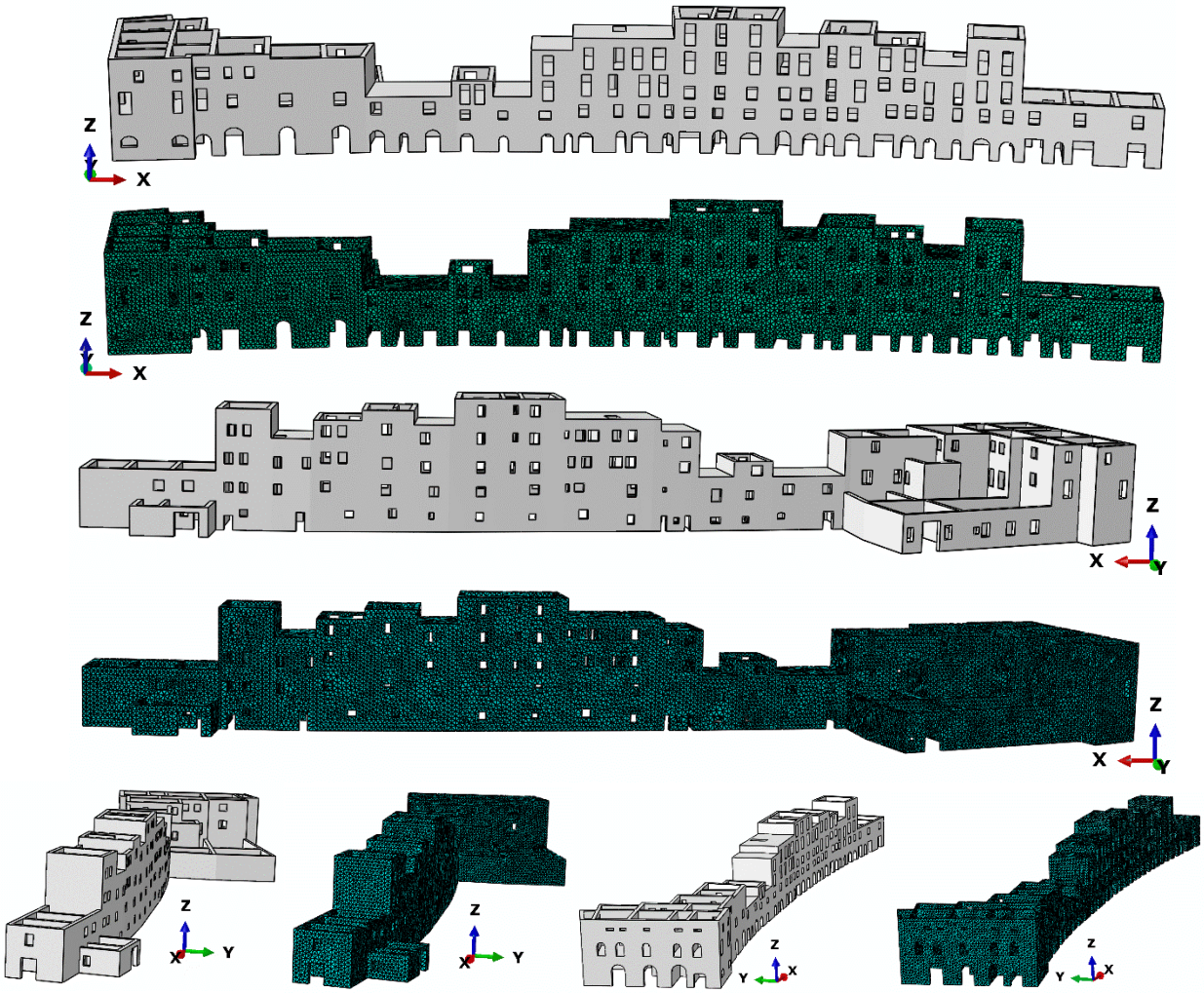

Figure 4. Geometrical and FE model of Aggregate 1: different views.

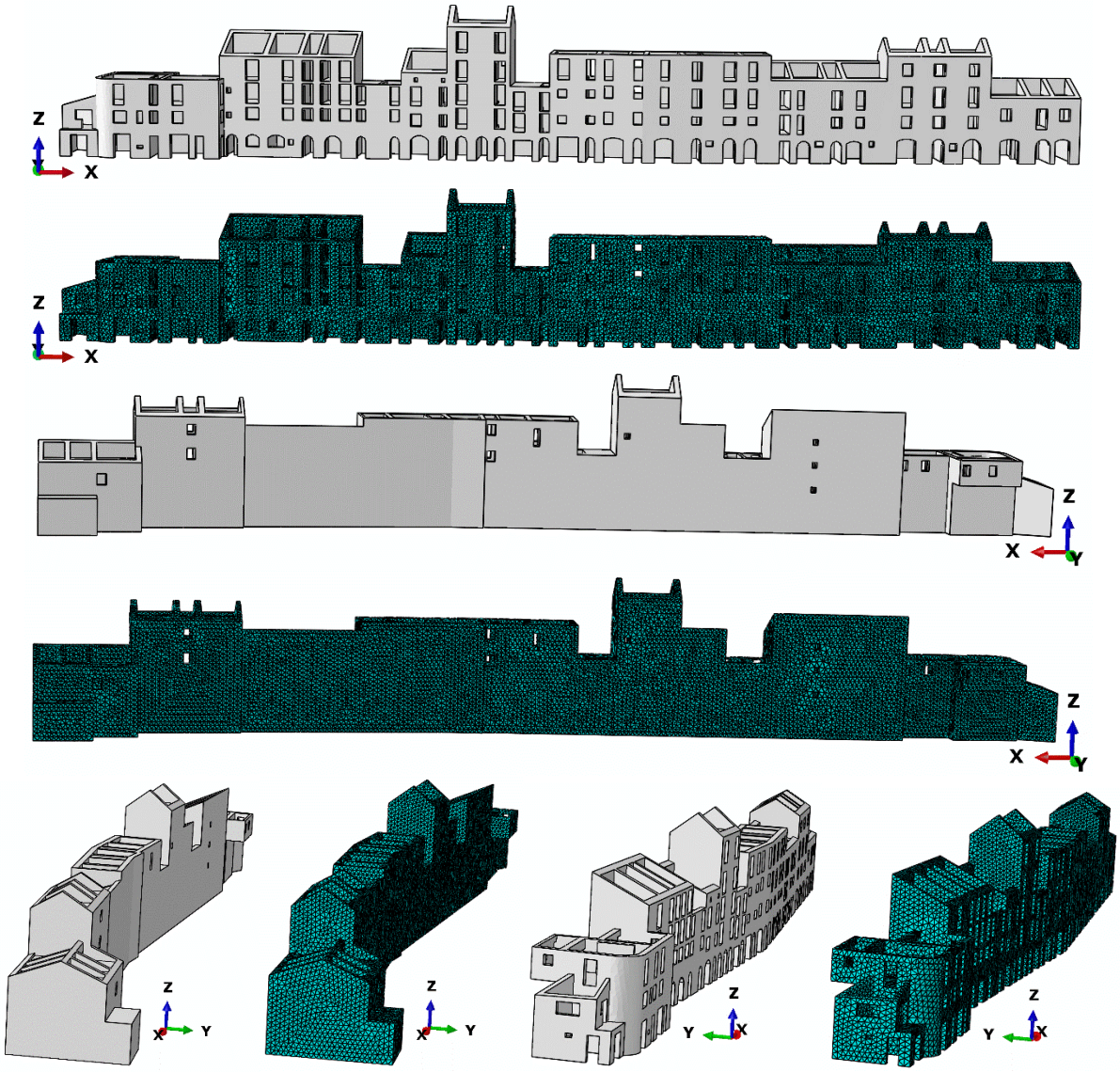

Figure 5. Geometrical and FE model of Aggregate 2: different views.

The concrete damaged plasticity (CDP) model is used to simulate the non-linear behavior of masonry in this study. Such a mechanical model, developed by Lubliner et al. [40] for concrete and further elaborated by Lee and Fenves [41], may be applied to materials with quasi-brittle behavior such as masonry. In particular, the CDP model has been already used to describe the seismic behavior of ancient masonry structures, see, among the others [42]-[48]. The model is characterized by linear and isotropic behavior in the elastic range and plastic damageable behavior in the non-linear range. It allows assigning different strength and distinct damage parameters in compression and tension, taking into account the softening once the material strength is reached, Figure 6: the main failure mechanisms are tensile cracking and compressive crushing.

The post-elastic behavior in tension and compression is described by uniaxial stress–strain relationships defining the uni-axial tensile σ_t and compressive σ_c stresses:

$$\sigma_t = (1-d_t)\,E_0\left(\varepsilon_t - \varepsilon_t^{pl}\right)$$
$$\sigma_c = (1-d_c)\,E_0\left(\varepsilon_c - \varepsilon_c^{pl}\right) \qquad (1)$$

where ε_t and ε_c are the total strain in tension and in compression, ε_t^{pl} and ε_c^{pl} are the equivalent plastic strain in tension and in compression, E_0 is the initial elastic modulus, and d_t and d_c are the scalar damage variables in tension and in compression.

Under cyclic loading conditions, the possible recovery of stiffness is expected in correspondence with a load reversal: such a recovery of stiffness is more pronounced as the stress state changes from tension to compression, causing tensile cracks to close. The stiffness recovery effects are taken into account with two parameters, w_c and w_t, as shown in Figure 6.

The CDP model uses a Drucker-Prager strength criterion that is modified through a parameter K representing the ratio of the second stress invariant on the tensile meridian to that on the compressive meridian: the value of the parameter K is set equal to 0.666, as suggested by the user's Guide of Abaqus [39]. The constitutive model is characterized by non-associated plastic flow condition. The dilation angle is assumed equal to 10°, in agreement with experimental data available in the literature. The flow potential eccentricity is set equal to 0.1, as suggested by the Abaqus user's Guide [39]. The ratio of initial biaxial compressive yield stress to initial uniaxial compressive yield stress is assumed equal to 1.16, in agreement with experimental results reported by Page [50] and then confirmed numerically in [51]. In order to obtain a visco-plastic regularization that improves the convergence of the model in softening conditions, a smoothing of the tension corner has been implemented through an eccentricity parameter equal to 0.002.

In this study, the same masonry material is assumed for all the units composing both the models in order to compare the global behavior of the two aggregates. This assumption can be adopted because the aggregates under study were built in the same period and belong to the same territorial area and, as previously pointed out, to focus the attention on the global behavior of aggregates and the interaction among the units. The main mechanical properties of masonry are assumed referring to the indications provided in the Italian recommendations for existing buildings and built heritage [11]-[13]. According to Table 8.2.1 in the Explicative Notes to the Italian code [12] the following assumptions are taken into account for a split stonework with good texture: (i) the density and the elastic modulus are equal to 2100 kg/m^3 and 1740 MPa, respectively; (ii) the compressive strength is equal to σ_{cu}=2.6 MPa. The tensile strength is assumed equal to σ_{to}=0.16 MPa, obtaining a ratio between the tensile and compressive strength equal to about 0.06. The compressive (d_c) and tensile (d_t) scalar damage variables, representative of the stiffness degradation of the material, are assumed to vary linearly: the values range from zero, for the strain corresponding to the stress peak, to 0.95, for the ultimate strain value of the softening branches.

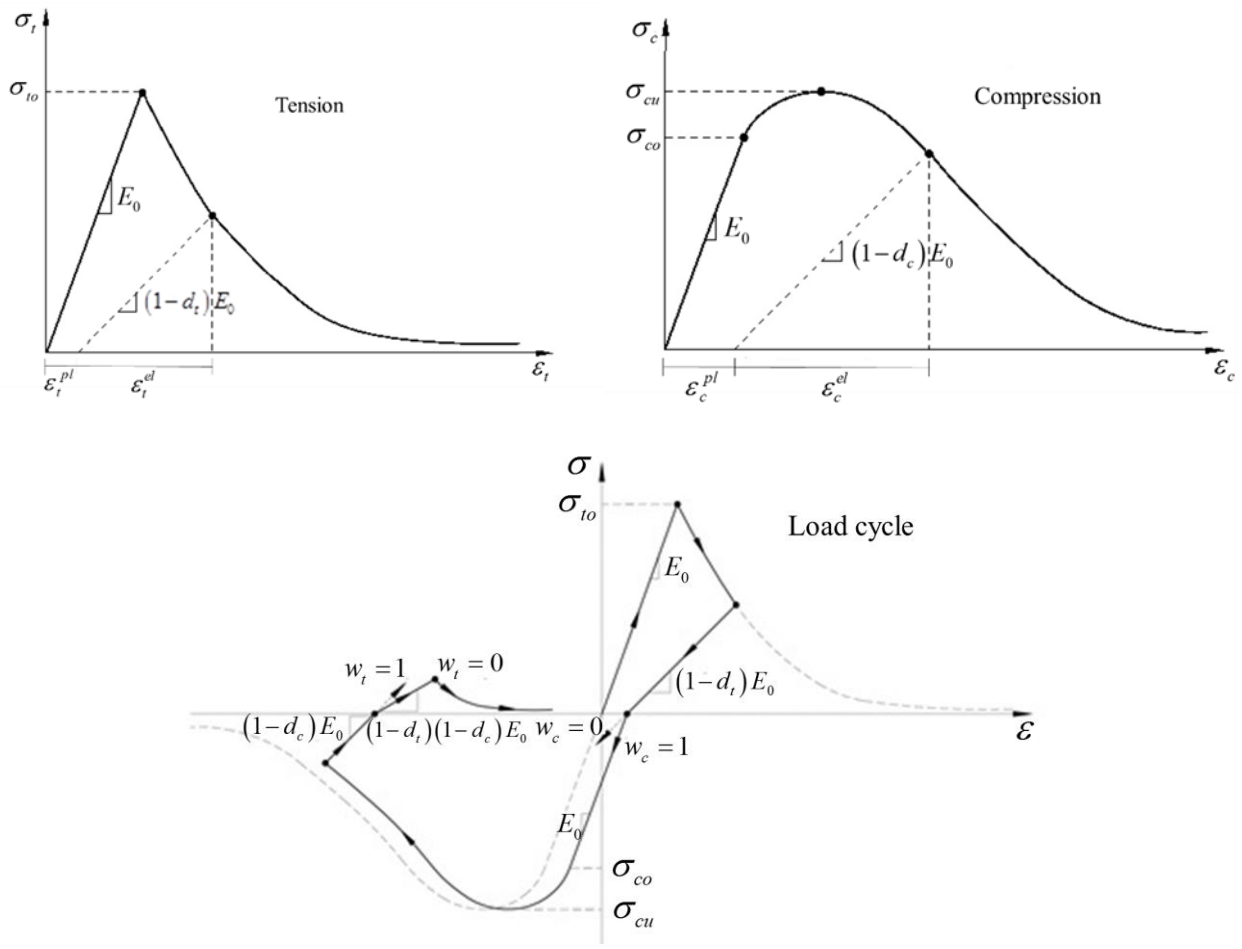

Figure 6. Stress-strain relationships of the CDP model: tension curve, compression curve and uniaxial load cycle (tension-compression-tension) response assuming different values for the stiffness recovery factors ($w_t = 0$ and $w_c = 1$).

The geometrical models of the two aggregates are subdivided into different macro-elements (walls), which are classified as perimeter walls facing north (N), east (E), south (S), west (W) and internal walls (I). Each perimeter macro-element generally coincides with a single perimeter wall of a unit and it is denoted by a number indicating the unit and a letter indicating the side: in the same way, each internal wall is denoted by the letter I and a progressive number. Figure 7 provides a schematic indication of the main walls in the geometrical models of the two aggregates. The subdivision into macro-elements allows identifying the local weaknesses of each structure and quantitatively comparing the seismic response of the two aggregates.

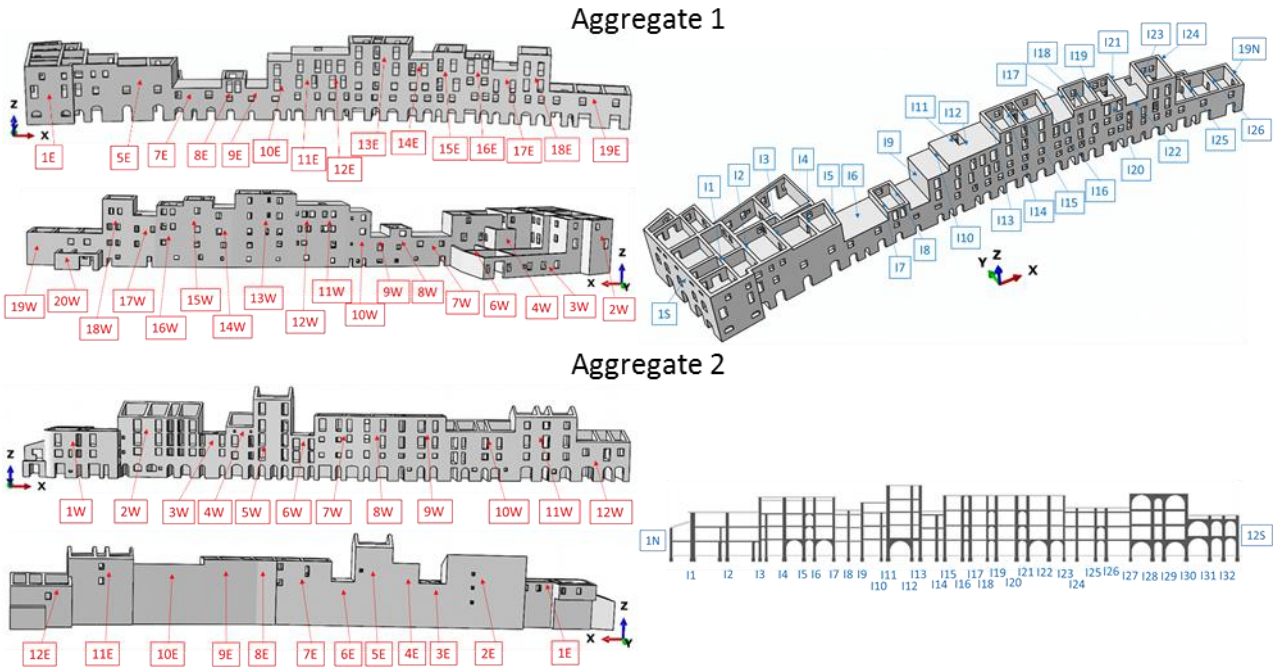

Figure 7. Schematic indication of the main walls in the FE models: Aggregate 1 (top) and Aggregate 2 (bottom).

4. Numerical analyses

Eigen-frequency analyses were conducted on the 3D FE models in order to obtain a preliminary insight into the dynamic behavior of the aggregates under study, identifying the main vibration modes, the corresponding periods and the participating mass ratios.

Whilst the results obtained have a strict numerical meaning, because they do not take into account that masonry is a damaging material with low tensile strength and pre-existing cracks patterns are disregarded, they provide an estimation of the most important natural frequencies and the corresponding excited mass. It is expected that, if the excited mass is not negligible and the period lays in the plateau range of the response spectrum, the activation of a failure mechanism described by the corresponding modal deformed shape can be active in the first instants of the application of the accelerogram [52]. In this regard, such an analysis provides useful hints for the subsequent application of limit analysis with pre-assigned failure mechanisms. Another interesting preliminary activity would be the determination of the experimental frequencies of the aggregate, with the subsequent structural identification. However, there was no possibility to perform such an experimentation to validate the numerical frequencies found. Moreover, many accelerometers should be used to experimentally estimate, with sufficient accuracy, the most important eigen-frequencies. It is an issue very difficult to tackle, also considering that there are only few papers available in the literature for the dynamic identification of palaces with complex geometry (see for example [53]), but nothing for aggregates, which are even more difficult to study.

The seismic response of the two aggregates was investigated through non-linear dynamic analyses using the real accelerogram registered on April 6 during the 2009 L'Aquila earthquake. Two different PGA values (PGA=0.15g and PGA=0.25g) were used in the non-linear dynamic analyses. It is worth mentioning that the highest values of the PGA used in the non-linear dynamic analyses approximately correspond to the maximum horizontal acceleration (ag) prescribed for that region at the Life Safety Limit State (SLV) according to Italian Code [11]-[13]. Figure 8 shows the two horizontal components of the acceleration time histories with PGA=0.25g applied in the longitudinal (north-south) and transversal (east-west) directions and the corresponding acceleration response spectra. The duration of the accelerograms was assumed equal to 10 s because of the high computational demand required

by the analyses. During the analyses the two horizontal components of the accelerograms have been applied simultaneously.
The tensile damage contour plots obtained at the end of the numerical simulations are shown for each aggregate; then, the maximum normalized displacements (top displacement/height) and the energy density dissipated by tensile damage (EDDTD) are reported for the main macro-elements (walls) of each aggregate.
The main aims of the numerical simulations are: (i) to describe the main features of the seismic response of such a typology of structures for which there is a lack of knowledge and information; (ii) to identify the most vulnerable elements of each aggregate; (iii) to assess and compare the damage evolution and the main response parameters variations of the two aggregates for different levels of seismic action.

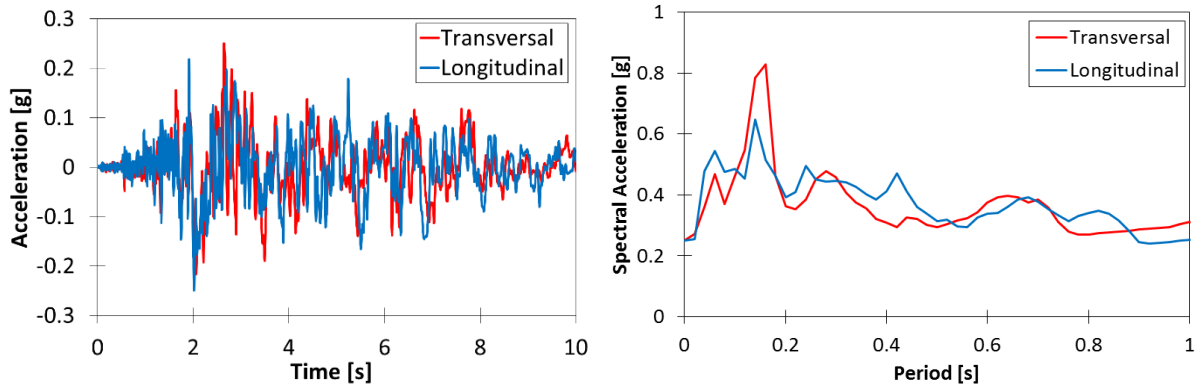

Figure 8. Accelerograms used in the non-linear dynamic analyses: north-south (longitudinal) component (blue) and east-west (transversal) component (red).

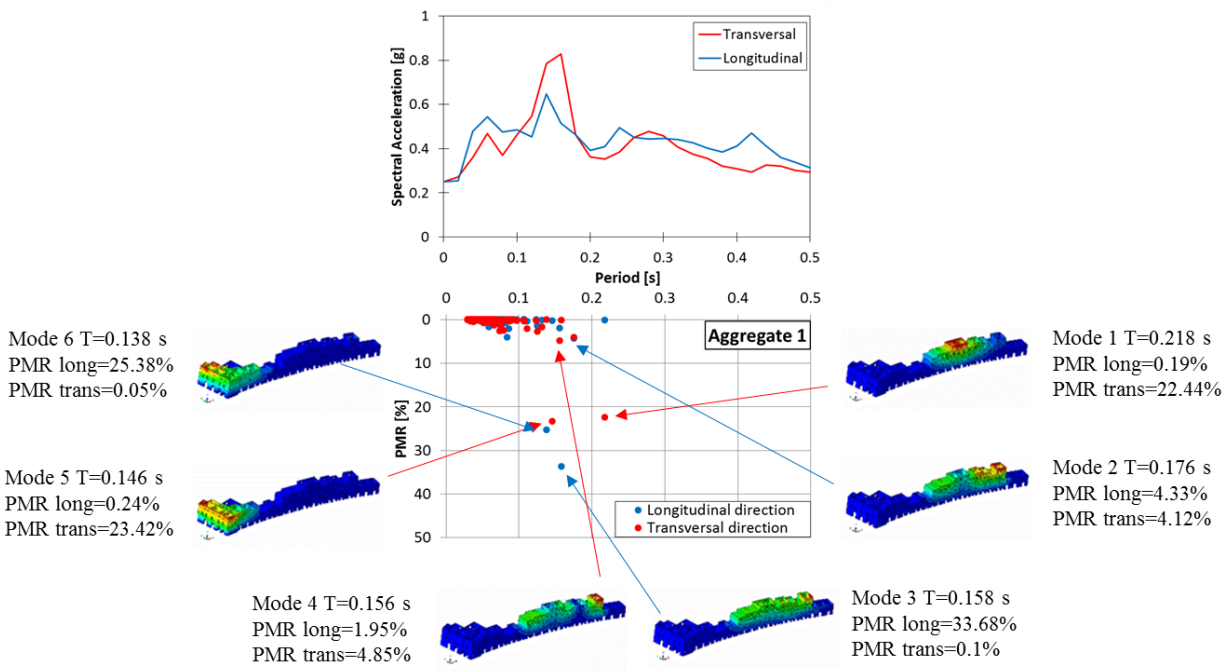

Figure 9. Aggregate 1. Distribution of the first three hundred modes in the longitudinal and transversal directions with reference to the response spectra of the accelerograms used in the non-linear dynamic analyses. Deformed shapes of the first six main modes, corresponding periods and participating mass ratios.

4.1. Aggregate 1

Figure 9 shows the deformed shapes and the corresponding periods of the main vibration modes with participating mass ratio (PMR) larger than about 4% for Aggregate 1: moreover, the distribution of the first three hundred modes in the longitudinal and transversal directions is presented with reference to the response spectra of the accelerograms used in the non-linear dynamic analyses.
The first four modes concern the central-northern part of the aggregate. In particular, the first mode (T=0.218 s) involves the central part of the aggregate with a significant PMR equal to about 22.4% in the transversal direction. The second mode (T=0.176 s) concerns the central part of the aggregate and the tallest unit in the northern part with a high torsional PMR. The third mode (T=0.158 s) involves the central part of the aggregate and the tallest unit in the northern part with the highest PMR equal to about 33.6% in the longitudinal direction. The fifth (T=0.146 s) and sixth (T=0.138 s) modes involve the southern extremity of the aggregate with a significant PMR equal to about 23.4% and 25.3% in the transversal and longitudinal directions, respectively. Considering the first three hundred modes, a cumulative participating mass ratio of about 89% in each horizontal direction is obtained.

Figure 10 and Figure 11 show the tensile damage contour plots for Aggregate 1 at the end of the non-linear dynamic analyses with PGA=0.15g and PGA=0.25g, respectively.
It can be observed that damage concentrates in the tallest units, in the central-northern part (U10-U18) and in the southern extremity, involving both the load-bearing walls and the floor/roof diaphragms: it has to be noted that the most damaged slabs and vaults are located in correspondence with the walls presenting extensive damage.
In detail, the non-linear dynamic analyses show the following significant damage concentrations.

- Severe damage, already marked under PGA=0.15g, is observed in the upper part of the tall unit U18 located in the northern part of the aggregate. Under PGA=0.25g, damage extends clearly also near the openings of the bottom stories. It is important to observe that in unit U18 damage is widespread both on the front and back sides. Considerable damage is registered also in the slabs of the upper stories, even under PGA=0.15g: damage concentrates mainly at the edges, in the connection regions with the walls. Moreover, it can be noted that the extensive damage observed in unit 18 spreads into the upper part of the adjacent unit U17.
- Significant damage is registered in the central part of the aggregate, mostly in units U10-U13. It can be noted that damage concentrates mostly in the front (east) side of the aggregate. The slabs of unit U10 are severely damaged at the second and roof stories, even under PGA=0.15g: damage concentrates at the edges, in the connection regions with the walls. Under PGA=0.25g, evident damage can be observed also on the front (west) side of units U14-U16.
- Widespread damage is registered in units U1-U2 located at the southern edge of the aggregate. Under PGA=0.15g, damage concentrates mostly on the back (east) side of the aggregate and in the wall facing south: under PGA=0.25g, significant damage can be observed also on the front (west) side and in the internal walls. Widespread damage can be observed in the slabs of unit U1, mainly at the second and roof storeys, even under PGA=0.15g: damage is uniformly distributed, indicating a probable collapse of the diaphragms.

It can be noted that in the central and northern parts damage is widespread especially from the second story upwards and concentrates mainly in correspondence with the openings, while in the southern extremity it is more distributed along the height of the structure: in particular, under PGA=0.25g, a clear damage concentration can be observed at the base of the wall facing south, indicating a probable overturning mechanism.

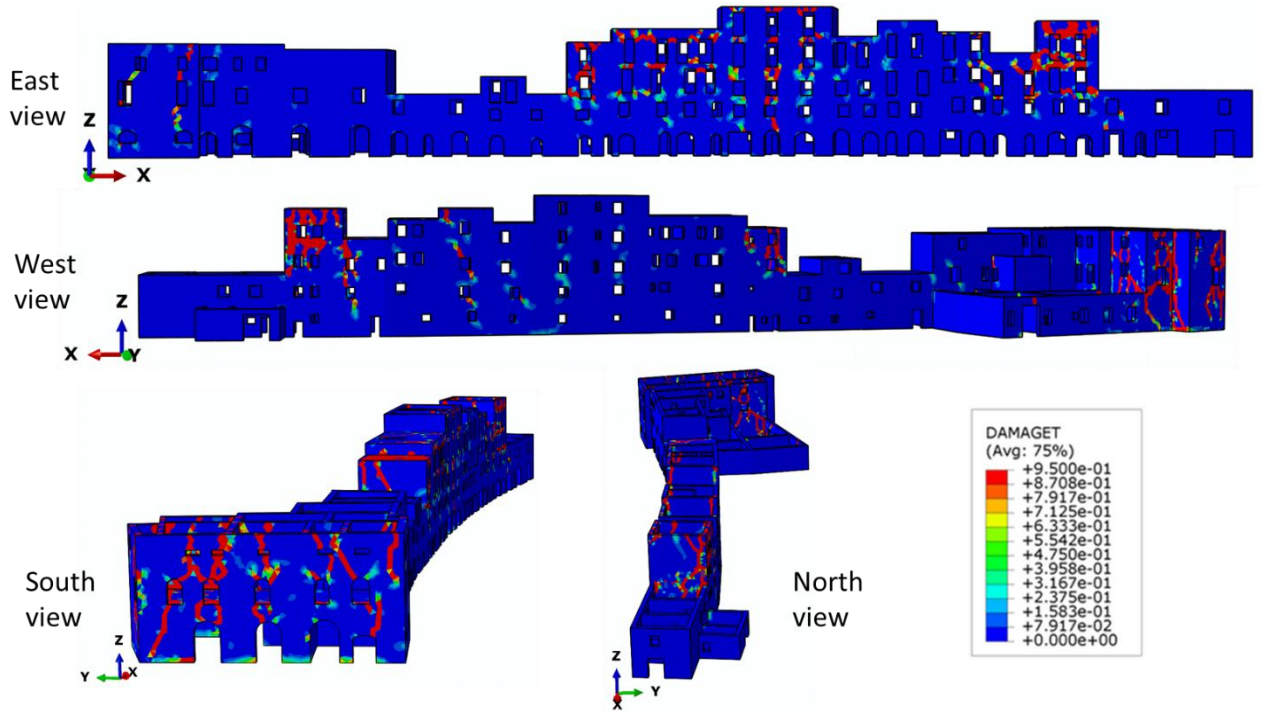

Figure 10. Aggregate 1: tensile damage contour plots at the end of the non-linear dynamic analysis with PGA=0.15g.

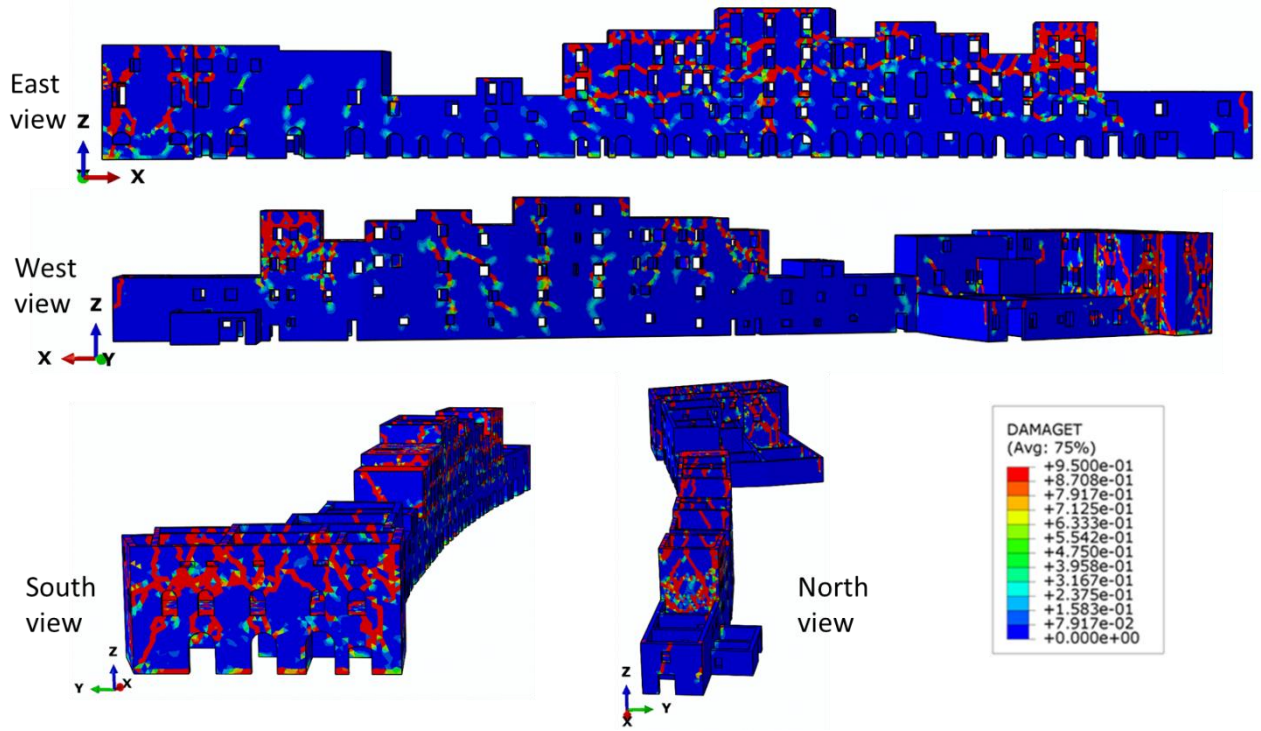

Figure 11. Aggregate 1: tensile damage contour plots at the end of the non-linear dynamic analysis with PGA=0.25g.

Figure 12 shows the maximum normalized displacements registered for the main walls of Aggregate 1 in the longitudinal (X) and transversal (Y) directions during the non-linear dynamic analyses with PGA=0.15g and PGA=0.25g: moreover, the walls exhibiting the largest normalized displacements under PGA=0.25g are schematically indicated in the aggregate.
The largest normalized displacements in the longitudinal (X) direction are registered for some internal walls and the south wall 1S (U1). In detail, three critical parts of the aggregate can be identified.

In the southern part, large normalized displacements (about 0.95%) are computed for the south wall 1S (U1) due to the lack of support from the adjacent slabs that present extensive damage: moreover, it is a perimeter wall that is prone to out-of-plane overturning due to the lack of support on the outside. The vulnerability of unit U1 is also enhanced by the presence of many openings on all the sides, and in particular on the south wall 1S. Normalized displacements larger than about 0.25% are also registered for the internal walls I5 (U5) and I1 (U1).

In the central part, normalized displacements larger than about 0.25% are computed for the internal wall I9 (U10). The lack of support from the adjacent unit, which is two storeys smaller, can lead to an overturning mechanism of the upper part; moreover, the vulnerability of such a wall is enhanced by the collapse of the adjacent slab at the fourth storey, resulting in a lack of support also on the other side.

In the northern part, large normalized displacements (about 0.7%) are registered for the internal wall I24 (U18) because it lacks supports from the adjacent unit, which is two storey smaller; moreover, the connections with the slabs of unit U18 are largely damaged and are ineffective to prevent an overturning mechanism. In addition, it should be noted that unit U18, similarly to the southern unit U1, is located at the extremity of the aggregate and consequently is subjected to high torsional effects induced by the seismic action. Normalized displacements larger than 0.32% are also registered for the internal wall I23 (U18).

The largest normalized displacements in the transversal (Y) direction are registered for some walls located on the west and east sides. In detail, three critical parts of the aggregate can be identified.

In the southern part, large normalized displacements (larger than about 0.6%) are computed for the west walls 1W (U1), 2W (U2) and the east wall 1E (U1). Such a result can be explained by both the peripheral position of such walls inside the aggregate and the lack of external supports: moreover, it can be noted that the slabs of units U1 and U2 are severely damaged.

In the central part, large normalized displacements (about 0.6%) are registered for the east wall 13E (U13) due to the lack of external support, the presence of several openings, the relevant height (larger than the nearby units) of the wall and the ineffective support provided by the internal slabs that are subjected to considerable damage. It has to be noted that normalized displacements larger than 0.35% are also computed for the east wall 10E (U10).

In the northern part, large normalized displacements (larger than about 0.35%) are computed for the east walls 18E (U18) and 19E (U19) and the west wall 18W (U18). In the case of unit U18, the out-of-plane displacement of the perimeter walls causes high deformations of the edges of the internal walls I23 and I24, which are vulnerable because they lack supports from the adjacent units: moreover, the connection regions with the slabs are severely damaged and thus ineffective to prevent out-of-plane displacements. It should be noted that such units (U18 and U19) are subjected to high torsional effects induced by the seismic action.

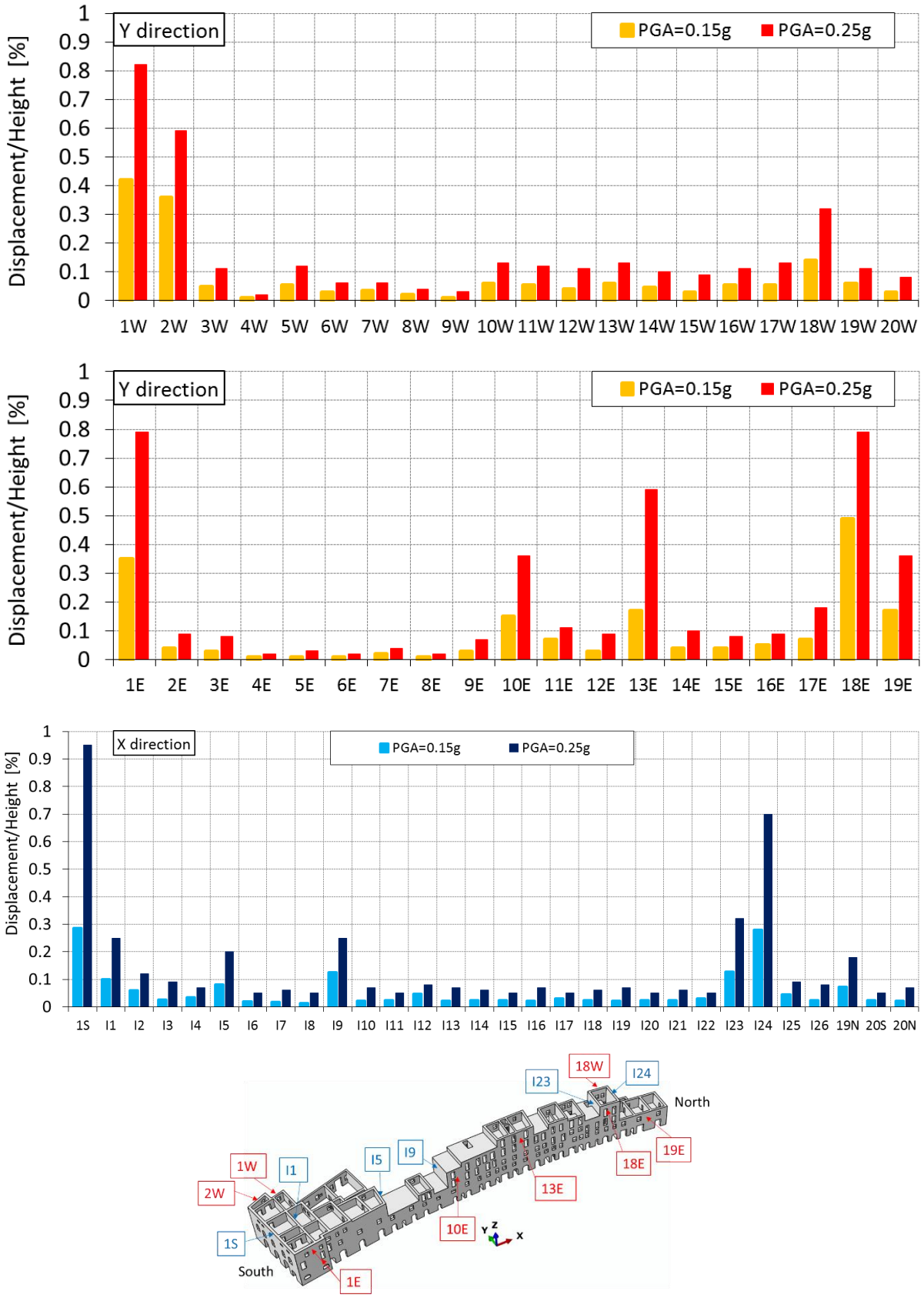

Figure 12. Aggregate 1: maximum normalized displacement registered for the main walls in the longitudinal and transversal directions during the non-linear dynamic analyses with different PGA.

Figure 13 shows the energy density dissipated by tensile damage (EDDTD) for the main walls of Aggregate 1 at the end of the non-linear dynamic analyses with PGA=0.15g and PGA=0.25g: moreover, the walls exhibiting the highest EDDTD values under PGA=0.25g are highlighted in the aggregate.

In the northern part, high EDDTD values are registered for the perimeter walls 18E and 18W of the tall unit U18: damage concentrates mainly in the upper part, which is not braced by the adjacent units, and especially close to the openings. Moreover, high EDDTD values are also observed for the internal walls I23 and I24 (U18), which exhibit notable damage along the whole height.

In the central part, high EDDTD values are registered for the east wall 10E (U10) and the internal wall I9: such a result may be correlated to the large displacements of the wall 10E and the extensive damage registered in the connection regions with the slabs: moreover, significant damage is observed at the base and near the openings of the upper part. It is important to highlight that high EDDTD values are also registered for the east tall wall 13E (U13): considerable damage is observed in the central part and close to the openings.

In the southern part, high EDDTD values are registered for the west walls 1W (U1) and 2W (U2), the internal wall I1 (U1), the east wall 1E (U1) and the south wall 1S (U1). In this portion of the aggregate, damage is distributed quite uniformly along the height with a clear concentration close to the openings. Significant damage is registered at the base of the south wall 1S (U1) and west wall 2W (U2), indicating an onset of possible overturning mechanisms. The high EDDTD value computed for the internal wall I1 (U1) could be correlated to the extensive damage observed in the connection regions with the slabs.

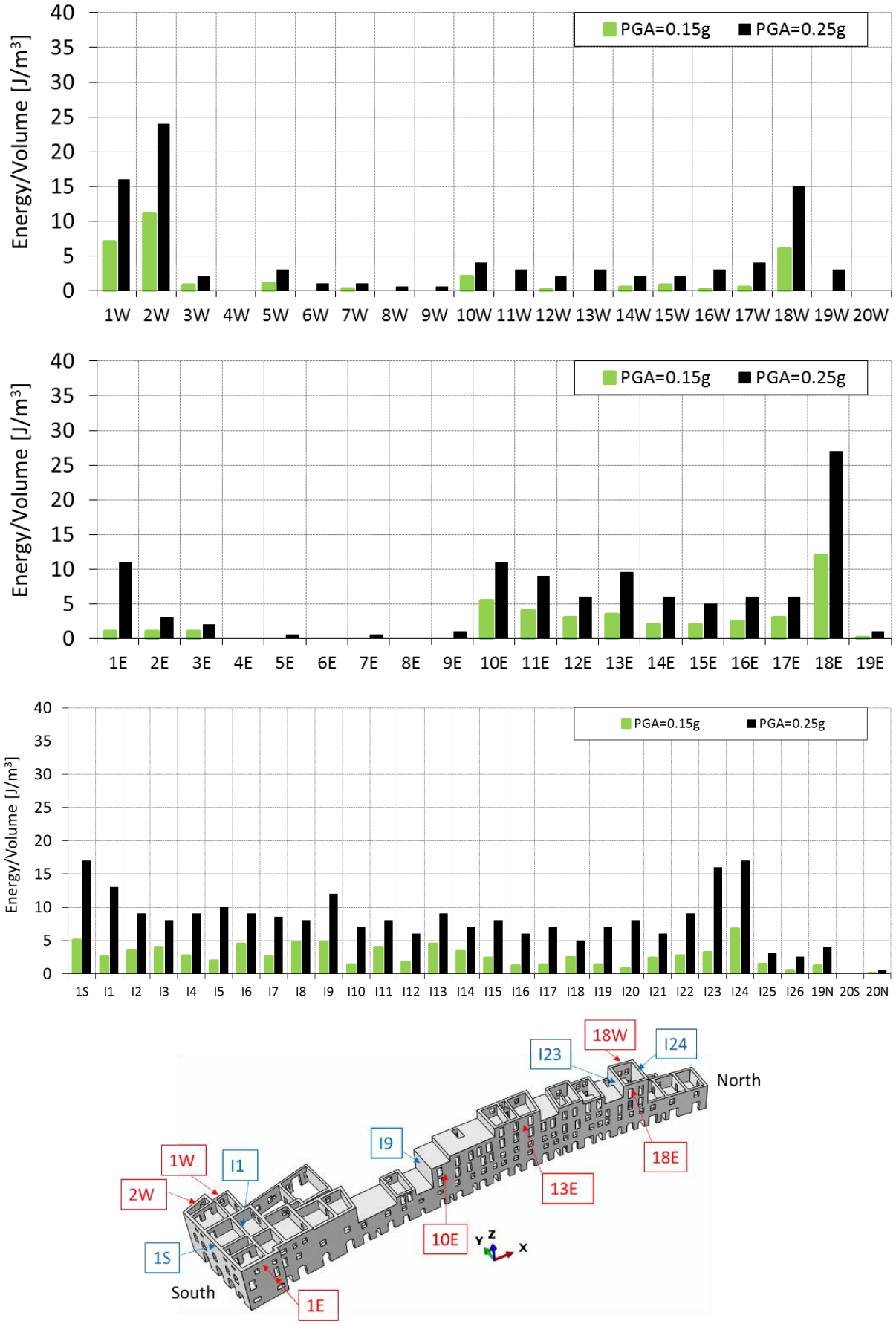

Figure 13. Aggregate 1: energy density dissipated by tensile damage (EDDTD) registered for the main walls at the end of the non-linear dynamic analyses with different PGA.

From the numerical results, the following observations can be summarized for the critical parts of Aggregate 1:

- In the southern part, the large displacements of the perimeter walls, which are prone to possible overturning mechanisms, and the extensive damage of the slabs at the upper floors result in significant damage also in the nearby walls and in the lower slabs. The out-of-plane displacements of the walls can weaken the wall-slab connections, as shown by the damage concentration at the edges of the slabs. Moreover, it is important to point out the small number of internal walls in such an extremity, which would provide higher stiffness and would reduce the spans and thus the deformation of the slabs.
- In the central part, the perimeter walls 13E and 10E exhibit large out-of-plane displacements due to the lack of lateral support, presence of several openings and the extensive damage observed in the wall-slab connections. Remarkable damage and large displacements are also observed for the internal wall I9, which lacks lateral support from the smaller adjacent unit.
- In the northern extremity, unit U18 can be identified as the critical one because all the four walls present significant damage as well as the internal slab at the fourth floor. The walls are particularly vulnerable due to their relevant height when compared with that of the small adjacent units.

4.2. Aggregate 2

Figure 14 shows the deformed shapes and the corresponding periods of the main vibration modes with participating mass ratio (PMR) larger than about 5% for Aggregate 2: moreover, the distribution of the first three hundred modes in the longitudinal and transversal directions is presented with reference to the response spectra of the accelerograms used in the non-linear dynamic analyses.
The first three modes concern different parts of the aggregate in the transversal direction. The first mode (T=0.267 s) involves the tallest unit of the aggregate with a PMR equal to about 12.6% in the transversal direction. The second mode (T=0.211 s) concerns the central-northern part of the aggregate with a PMR equal to about 6.5% in the transversal direction and a significant torsional component. The third mode (T=0.204 s) involves the central-southern part of the aggregate with a significant PMR equal to about 30.8% in the transversal direction and a significant torsional component. The fifth mode (T=0.167 s) concerns the tallest unit in the central part of the aggregate with a PMR equal to about 7.2% and 7.1%, respectively, in the longitudinal direction. The ninth mode (T=0.135 s) involves the tallest block in the southern zone of the aggregate with the highest PMR equal to about 37.8% in the longitudinal direction. The eleventh mode (T=0.121 s) involves the central-northern zone of the aggregate with a PMR equal to about 10.9% in the longitudinal direction. Considering the first three hundred modes, a cumulative participating mass ratio of about 90% in each horizontal direction is obtained.

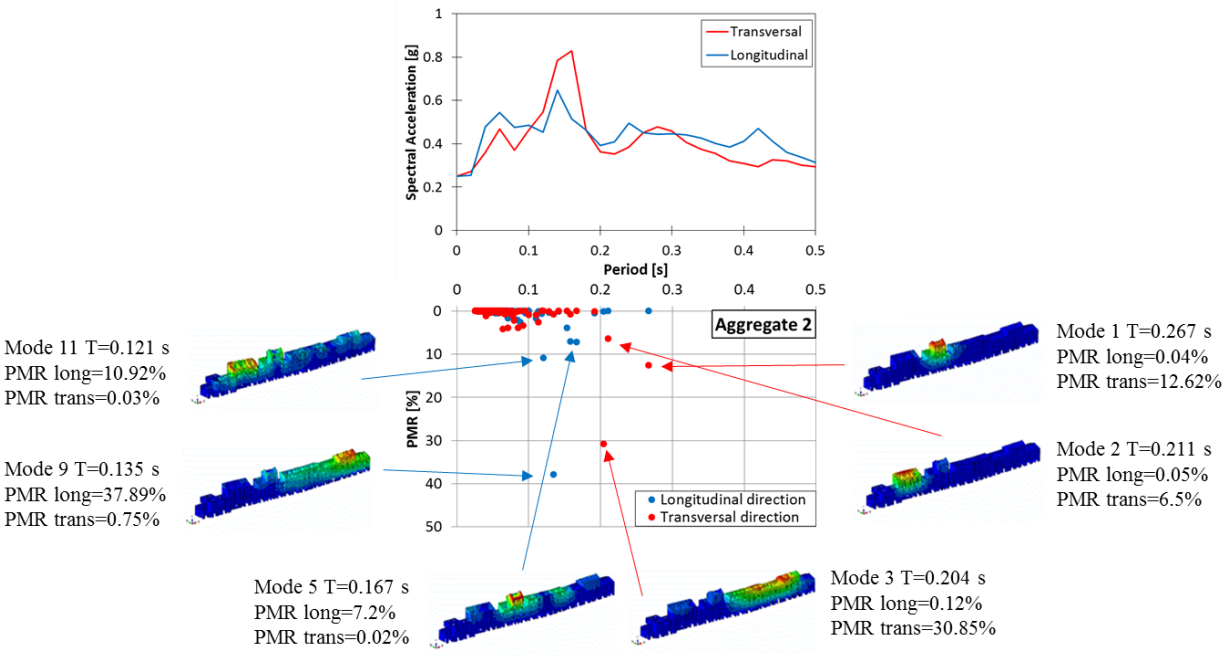

Figure 14. Aggregate 2. Distribution of the first three hundred modes in the longitudinal and transversal directions with reference to the response spectra of the accelerograms used in the non-linear dynamic analyses. Deformed shapes of the first six main modes, corresponding periods and participating mass ratios.

Figure 15 and Figure 16 show the tensile damage contour plots for Aggregate 2 at the end of the non-linear dynamic analyses with PGA=0.15g and PGA=0.25g, respectively. It can be observed that damage concentrates in the tallest units, in the northern extremity (U1-U2), in the central-northern part (U3-U6) and in the southern extremity (U10-U12) for both the PGA values: moreover, the most damaged slabs and vaults are located in correspondence with the walls presenting extensive damage. In detail, the results of the non-linear dynamic analyses show the following significant damage concentrations:

- Notable damage, already visible under PGA=0.15g, is registered in the front (west) side of units U1-U2 located in the northern extremity of the aggregate: several marked cracks are observed mostly in correspondence with the openings. The diaphragms of units U1-U2 exhibit considerable damage, mainly in the connection regions with the walls.
- Significant damage, already marked under PGA=0.15g, is observed in the central-northern part of the aggregate, mainly in the front (west) side of units U5-U6. Under PGA=0.25g, relevant damage appears also in units U3-U4 and a more widespread damage is detected in the upper part of the back (east) side of unit U5. The diaphragms of units U5-U6 present extensive damage.
- Widespread damage, already marked under PGA=0.15g, is registered in units U10-U12 located in the southern extremity: under PGA=0.25g damage increases involving also unit U9. Several marked cracks are observed mostly in correspondence with the openings. In such units the diaphragms exhibit significant damage mainly at the edges, in the connection regions with the bearing walls.

It is important to observe that widespread damage is visible mainly in the front (west) side of the aggregate. Minor damage is observed in the back (east) side, with some exceptions: the southern extremity (units U11-U12) and the central-northern part (units U5-U6). Moreover, it can be noted that in the central and northern parts clear damage is visible especially from the first storey upwards and concentrates mostly in correspondence with the openings. In the southern extremity damage is distributed more uniformly on the whole height, including the back (east) side.

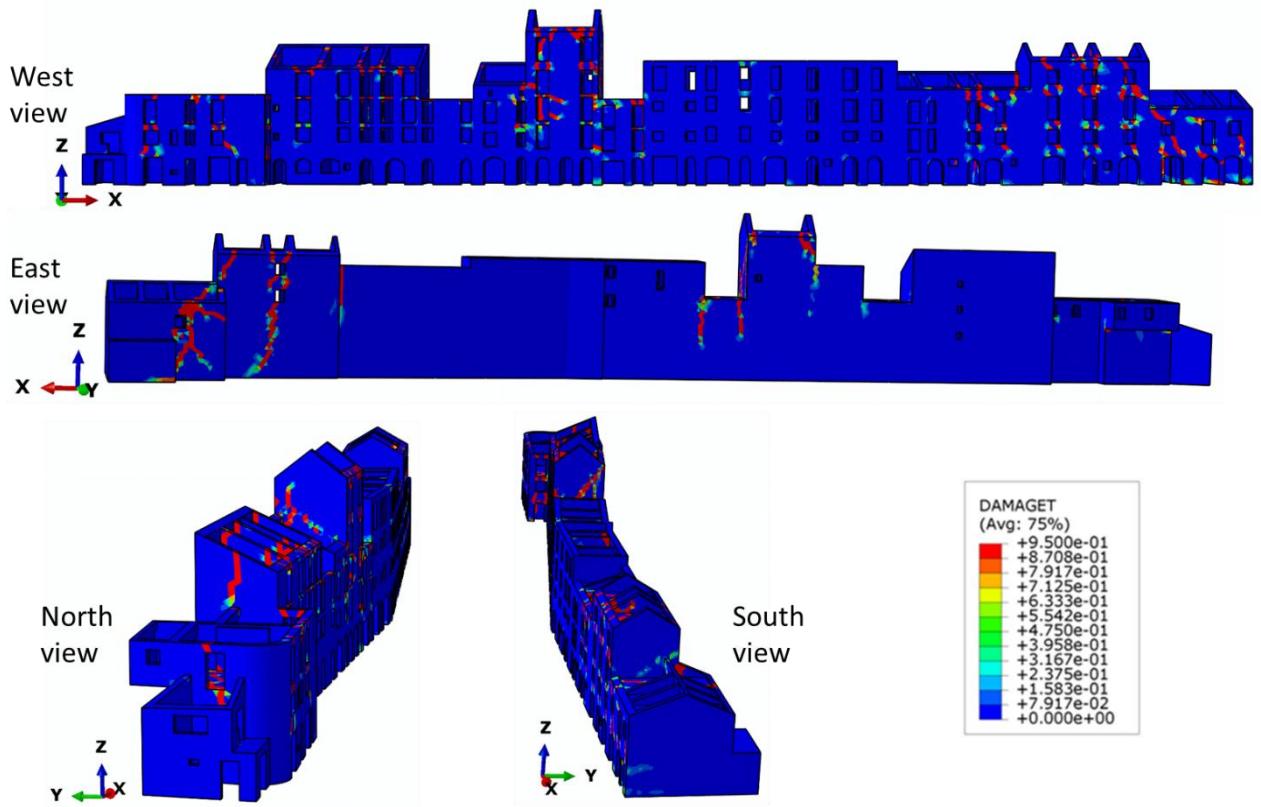

Figure 15. Aggregate 2: tensile damage contour plots at the end of the non-linear dynamic analysis with PGA=0.15g.

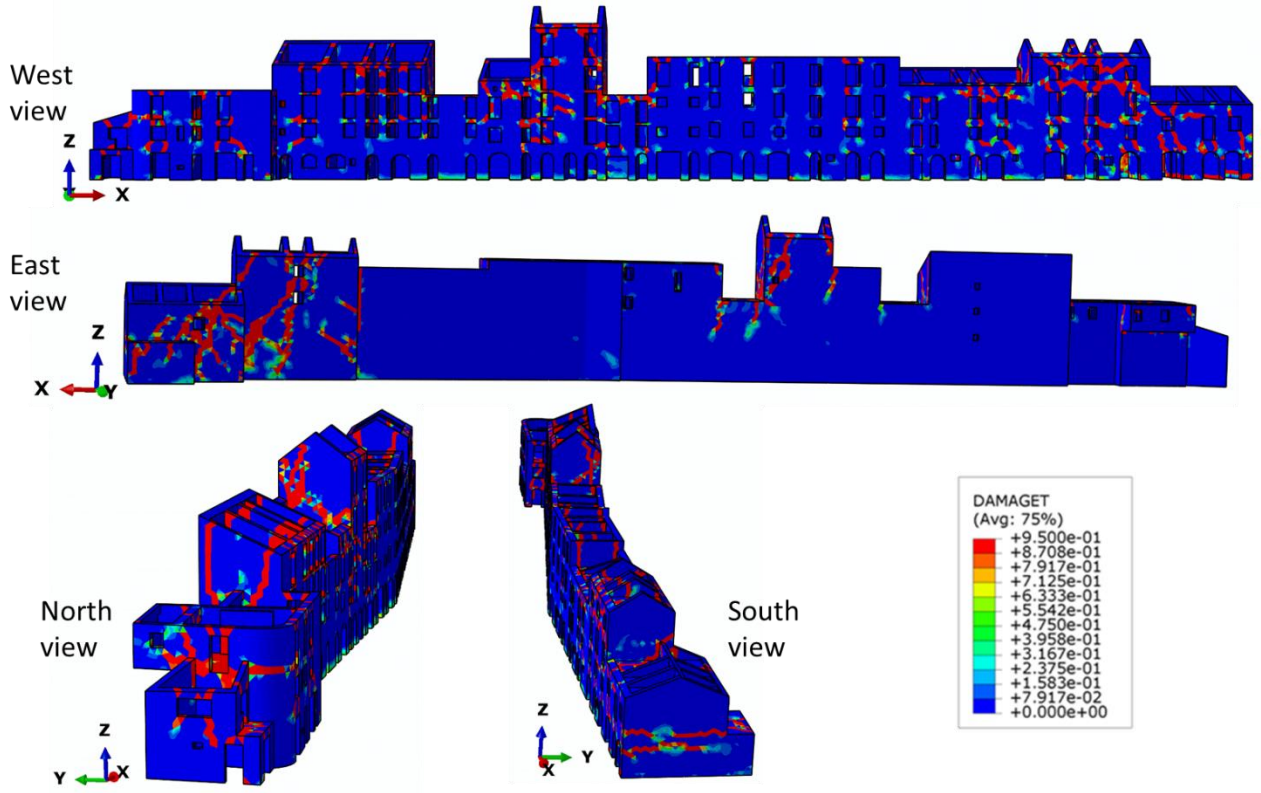

Figure 16. Aggregate 2: tensile damage contour plots at the end of the non-linear dynamic analysis with PGA=0.25g.

Figure 17 shows the maximum normalized displacements registered for the main walls of Aggregate 2 in the longitudinal (X) and transversal (Y) directions during the non-linear dynamic analyses with PGA=0.15g and PGA=0.25g: moreover, the walls exhibiting the largest normalized displacements under PGA=0.25g are schematically indicated in the aggregate.
The largest normalized displacements in the longitudinal (X) direction are registered at the top of some internal walls and three critical parts of the aggregate can be identified.

In the northern part, large normalized displacements (about 0.3%) are computed for the internal wall I3 (U1) due to the lack of support from the adjacent smaller unit and the extensive damage observed in the connection regions with the internal slabs. Normalized displacements larger than 0.25% are also observed for the internal walls I5, I6, I7 of unit U2.

In the central part, large normalized displacements (about 0.5% and 0.75%, respectively) are registered for the internal walls I11 and I13 (U5), which are two storeys higher than the adjacent units and consequently lack external supports in the upper part; in addition, the internal slabs present widespread damage in the connection regions.

In the southern part, large normalized displacements (about 0.4%) are registered for the internal wall I30, which is the south wall of the tall unit U11 and lacks support from the smaller edge unit U12 of the aggregate. Normalized displacements larger than about 0.3% are computed also for the internal wall I27, which is the north wall of U11 and is not braced by the smaller adjacent unit U10, and for the edge south wall 12S (U12), which is also subjected to high torsional effects induced by the seismic action.

The largest normalized displacements in the transversal (Y) direction are computed for some walls located on the west and east sides, defining three critical parts of the aggregate. Moreover, it can be noted that the walls on the east side, which are characterized by very few openings, present smaller displacements than the walls on the west side.

In the northern part (U1-U2), large normalized displacements (0.55% and 0.3%, respectively) are computed for the west walls 1W (U1) and 2W (U2) that can be subjected to a possible overturning mechanism. It can be noted that the west wall 1W presents several openings and the connection regions with the internal slabs are largely damaged. The west wall 2W (U2) exhibits several openings and is prone to a possible overturning mechanism considering the significant damage at the edges of the internal walls. Both the walls are subjected to high torsional effects due to the seismic action.

In the central part (U5-U6), large normalized displacements (about 0.45%) are registered for the west walls 5W (U5) that can be subjected to a possible overturning mechanism: it can be noted that such a wall belongs to the tall unit 5, which presents severe damage in the connection regions with the internal slabs. Moreover, normalized displacements larger than 0.2% are computed for the adjacent west wall 6W (U6) that exhibits several openings.

In the southern part (U11-U12), normalized displacements larger than about 0.3% are registered for the west walls 11W and 12W (U11-U12) and the east walls 11E and 12E (U11-U12), which can be prone to a possible overturning mechanism. Such perimeter walls are characterized by several openings and are subjected to high torsional effects induced by the seismic action.

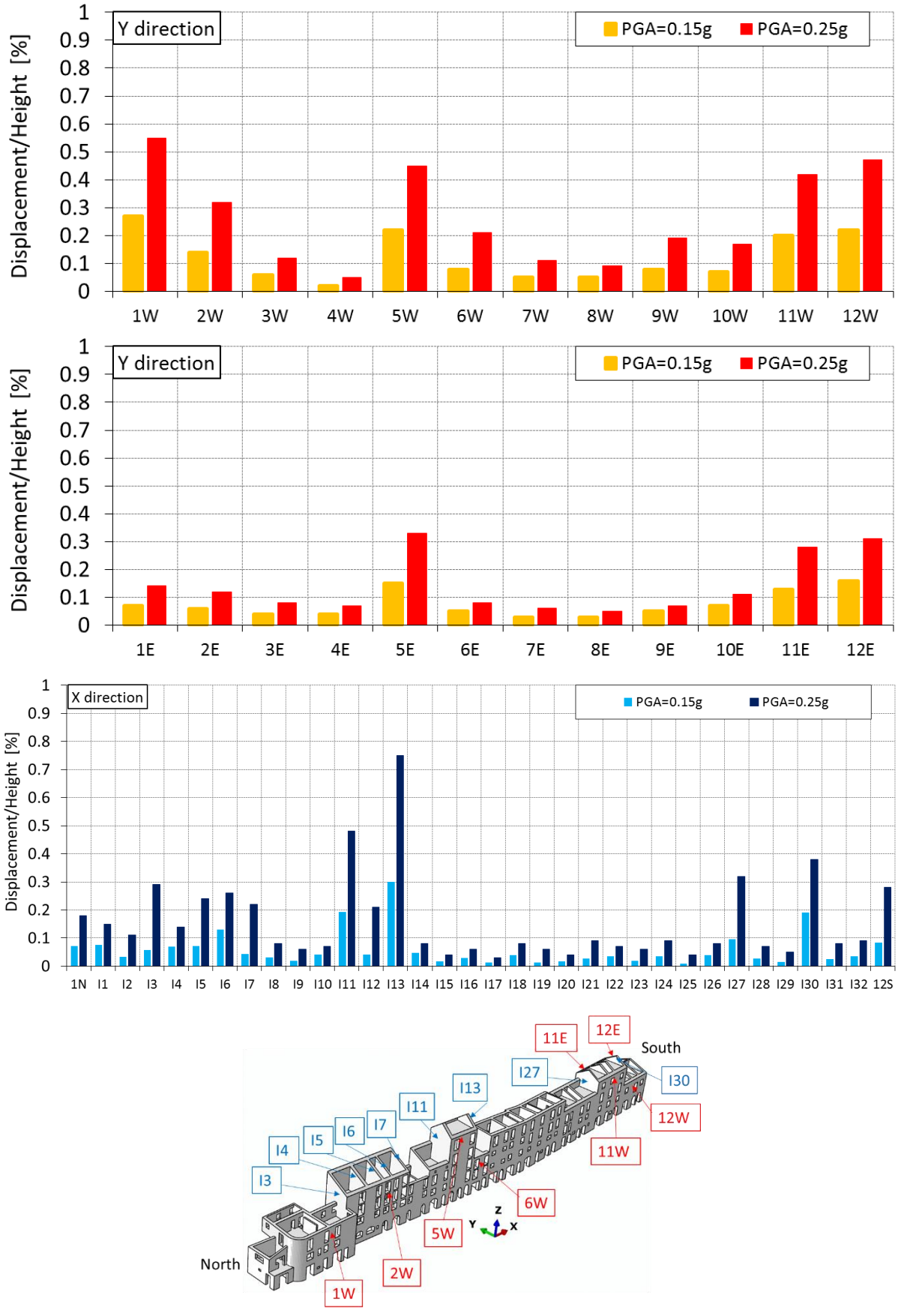

Figure 17. Aggregate 2: maximum normalized displacements registered for the main walls in the longitudinal and transversal directions during the non-linear dynamic analyses with different PGA.

Figure 18 shows the energy density dissipated by tensile damage (EDDTD) for the main walls of Aggregate 2 at the end of the non-linear dynamic analyses with PGA=0.15g and PGA=0.25g: moreover, the walls exhibiting the highest values of EDDTD under PGA=0.25g are schematically indicated in the aggregate.

In the northern part (U1-U2), high EDDTD values are registered for the internal walls (I3, I4, I5, I6, I7) of unit U2. Damage concentrates mainly in correspondence with the east wall, the openings and the connection regions between the walls and the slab. In addition, it can be noted that such walls present damage from the first storey upwards, while the lower part exhibits negligible damage. High EDDTD values are observed for the west walls 1W and 2W, which exhibit damage mainly close to the openings.

In the central part (U5-U6), high EDDTD values are registered for the west wall 5W, which presents significant damage around the openings and at the base, and for the east wall 5E. High EDDTD values are computed also for the internal walls I11 and I13, which exhibit marked damage in the middle part and in the connection regions with the diaphragms. High EDDTD values are observed for the west wall 6W, which shows relevant damage near the openings and at the base.

In the southern part (U11-U12), high EDDTD values are registered for the internal walls I27 and I30 (U11). Damage concentrates around the openings and, in the case of wall I30, in the connection regions with the east wall. High EDDTD values are observed for the east walls 11E and 12E and the west walls 10W, 11W and 12W: the east walls present substantial damage along the whole height, while the west walls exhibit notable damage around the openings and at the base.

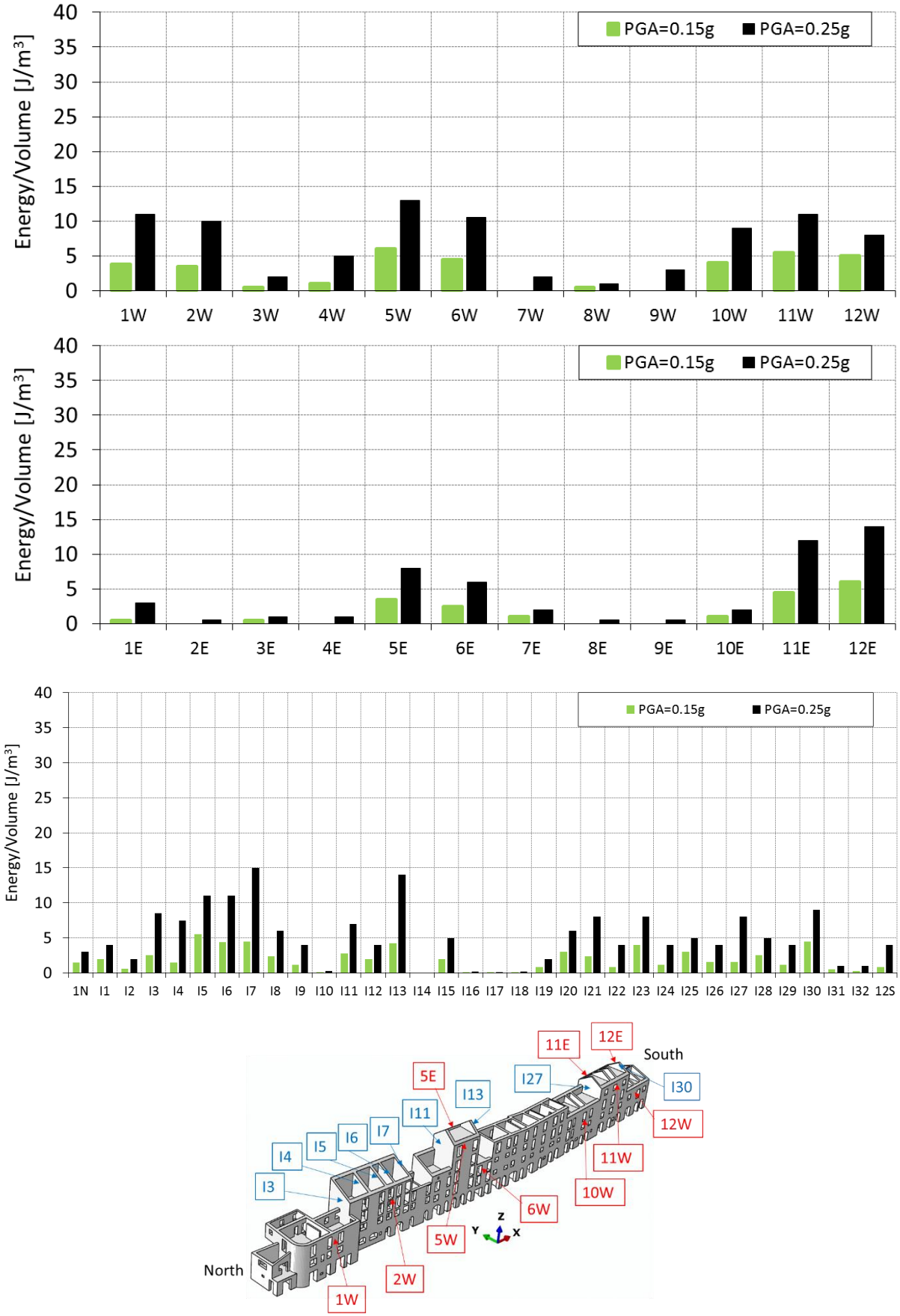

Figure 18. Aggregate 2: energy density dissipated by tensile damage (EDDTD) registered for the main walls at the end of the non-linear dynamic analyses with different PGA.

From the numerical results, the following observations can be summarized for the critical parts of Aggregate 2:

- In the northern part, the perimeter wall 1W presents large displacements in the transversal direction: it can be noted that the adjacent slabs are characterized by large spans and present significant damage in the connection regions with the wall. In unit U2, the internal walls are subjected to relevant displacements and notable damage in the upper part. Moreover, the possible overturning mechanism of the west wall 2W generates significant damage at the edges of the internal walls.
- The central part presents large displacements and considerable damage in correspondence with the tall unit U5. The absence of lateral supports and the extensive damage in the slabs and in the connection regions with the walls favors the out-of-plane displacements of the perimeter and internal walls. It can be noted that the bottom part of the unit is strengthened by the presence of a barrel vault, while the upper part, where the slabs are severely damaged, shows relevant damage and displacements.
- In the southern extremity, the east and west walls present large normalized displacements in the transversal (Y) direction: the out-of-plane displacements of the perimeter walls create a remarkable damage concentration at the edges of the internal walls.
- Comparing the different response of the west and east sides, it can be noted that the presence of openings significantly increases both the normalized displacements and damage level of the perimeter walls.

5. Comparison and discussion of the numerical results

The results of eigen-frequency analyses indicate that the first main modes of both the aggregates involve mainly the tallest units: moreover, the transversal direction is the critical direction for both the aggregates, especially for Aggregate 2. On the basis of the damage observed during the following non-linear dynamic analyses, it can be affirmed that eigen-frequency analysis may represent a fast and useful tool to provide a preliminary assessment of the structural weaknesses and deficiencies of the aggregates. Moreover, it can be noted that low values of PMR are associated with the main modes: as a result, a large number of modes should be considered to reach significant effective modal masses and thoroughly describe the global response of the aggregates. In addition, it is important to observe that similar low values of period are registered for the first main modes of the two aggregates: in fact, for both the aggregates the modes characterized by high PMR present low values of period, which correspond to high amplifications of the spectral acceleration.

Figure 19 shows the evolution of the global energy density dissipated by tensile damage (EDDTD) for the two aggregates during the non-linear dynamic analyses with different PGA. A large increase of EDDTD can be observed in the case of PGA=0.25g for both the aggregates. Moreover, it can be noted that the EDDTD values are larger in Aggregate 1 than in Aggregate 2. In fact, the low damage level on the back side of Aggregate 2 results in smaller values of EDDTD when compared to Aggregate 1. Such a difference is mainly due to the higher number of openings on the back side of Aggregate 1 than that of Aggregate 2, because considerable damage tends to concentrate in correspondence with openings.
For Aggregate 1 the maximum EDDTD values are registered for the perimeter east wall 18E located in the northern part and the perimeter west wall 2W located in the southern part. For Aggregate 2 the maximum EDDTD values are registered for some internal walls (I7 and I13) and the west wall 5W of the tall units and the east wall 12E of the southern extremity.

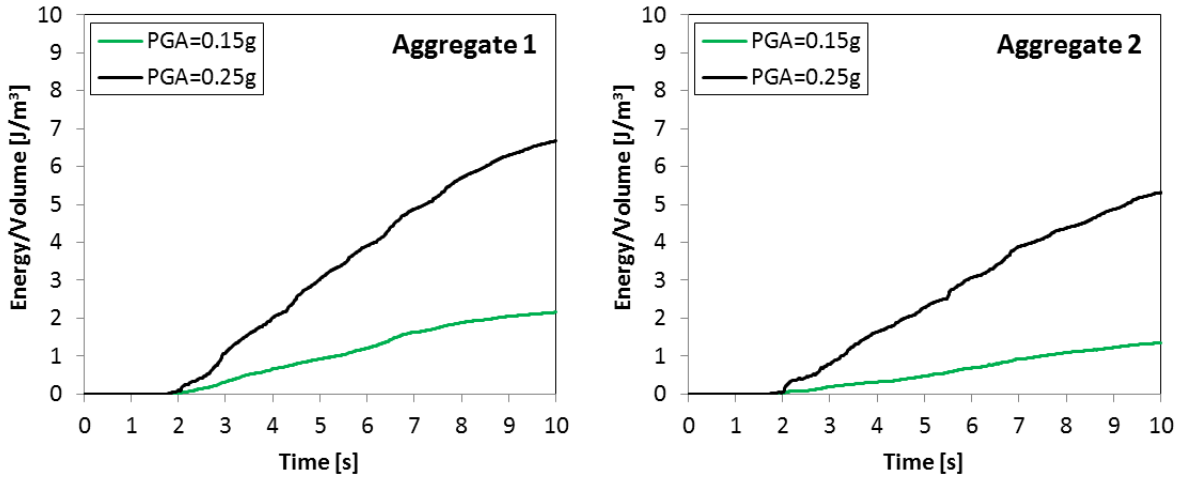

Figure 19. Energy density dissipated by tensile damage (EDDTD) registered for the two aggregates during the non-linear dynamic analyses with different PGA: Aggregate 1 (left) and Aggregate 2 (right).

Figure 20 shows the maximum normalized base shear (base shear/weight) in the two orthogonal directions registered for the two aggregates during the non-linear dynamic analyses with different PGA. The highest values of the normalized base shear are observed in the longitudinal direction for both the aggregates, as could be derived from the preliminary results of the modal analysis indicating a lower stiffness in the transversal direction. Moreover, it can be noted that the values of the normalized base shear are larger for Aggregate 1 under PGA=0.15g and for Aggregate 2 under PGA=0.25g.

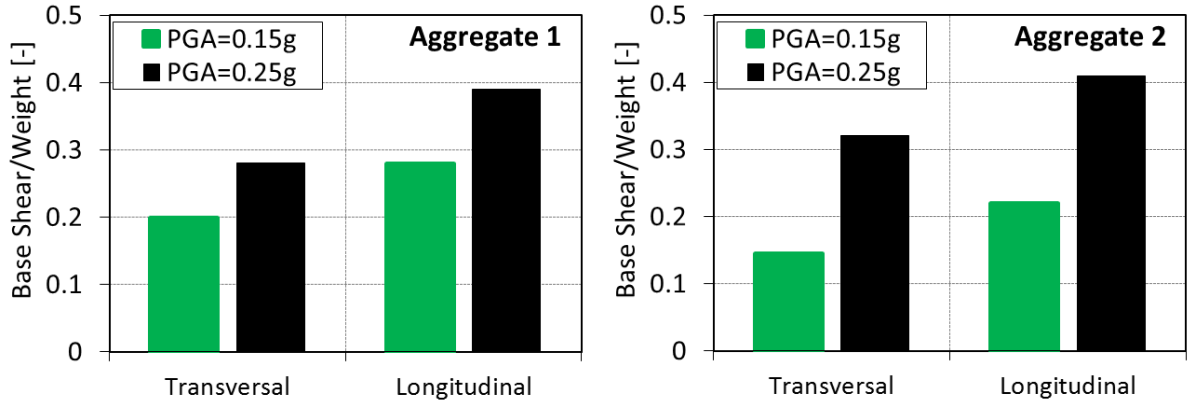

Figure 20. Maximum base shear/weight ratio registered for Aggregate 1 (left) and Aggregate 2 (right) in the transversal and longitudinal directions during the non-linear dynamic analyses with different PGA.

For both the aggregates, the structural response of a unit is strongly affected by the adjacent units. As regards the damage distribution, for both the aggregates the walls present significant damage mainly in correspondence with the openings, in the connection regions with the slabs and the orthogonal walls. Some critical perimeter walls exhibit marked damage also at the base, indicating the probable occurrence of an overturning mechanism: such a result is generally related to extensive damage in the connection regions with the slabs. The tallest units and the units at the extremities are the most damaged portions for both the aggregates. In Aggregate 1 extensive damage is registered both on the front and back sides, while in Aggregate 2 damage concentrates mainly on the front side because the back side does not present openings.

Significant damage can be observed in the floor and roof diaphragms of the critical units of the aggregates: it can be noted that the most critical diaphragms present wide span and belong to the tallest units. In both the aggregates, the diaphragms with extensive damage are generally subjected to large vertical displacements or are located near the walls presenting high horizontal displacements. Damage generally concentrates at the edges, in the connection regions with the walls. It can be noted that Aggregate 2 presents more barrel vaults than Aggregate 1, both at the ground floor and in the upper part; damage is generally reduced in the case of barrel vaults. The covering in the southern part of Aggregate 1 present more significant damage than those of Aggregate 2, due to the larger span and smaller number of vaults.

For both the aggregates the largest normalized displacements in the longitudinal (X) direction are computed for the internal transversal walls of the tallest units, which are not efficiently braced by the smaller neighboring units, or the transversal walls located at the extremities of the aggregate, which lack lateral support from the adjacent units. For Aggregate 1 the largest displacements are registered for the south wall 1S located in the southern part and the internal wall I24 located in the northern part. For Aggregate 2 the largest displacement is registered for the internal wall I13 located in the central part.

For both the aggregates the walls subjected to the largest displacements in the transversal (Y) direction are the perimeter walls that may be prone to possible overturning mechanisms due to the lack of external supports. It can be noted that the walls facing Borgo San Rocco street (east walls for Aggregate 1 and west walls for Aggregate 2) are more critical because they are characterized by several openings. Moreover, it is important to observe that for both the aggregates the largest displacements are computed for the walls of the tallest units, in presence of extensive damage in the connection regions with the slabs and vaults, and the walls at the extremities of the aggregate, where the torsional effects induced by the seismic actions are larger. For Aggregate 1 the largest displacement is registered for the perimeter east walls 1E and 18E located at the two extremities and the perimeter west wall 1W located in the southern extremity. For Aggregate 2 the largest displacement is registered for the west walls 1W and 12W at the two extremities.

The presence of deformable floors, as already pointed out, is certainly responsible for the activation of partial failure mechanisms, with the collapse of portions of the most vulnerable units for out-of-plane overturning.
Kinematic limit analysis applied on out-of-plane pre-assigned failure mechanisms is certainly the most straightforward approach that can be used in practice to quickly estimate the horizontal acceleration associated with the activation of the first failure mechanisms. It is extremely useful for practitioners, because they certainly do not have the possibility (and the sufficient know-how) to perform complex and demanding non-linear dynamic analyses.
Alternative simplified procedures are possible, as for instance the possibility to apply the methodology recommended by the Italian guidelines for cultural heritage for palaces [13]. However, such a procedure is a revisited POR method that must be considered as a global approach where piers are modeled with mono-dimensional elements. The presence of wooden floors with insufficient stiffness promotes the activation of out-of-plane failure mechanisms, therefore the utilization of models based on equivalent frame assumptions may be considered questionable in their capability to predict the real behavior at collapse. Such a discussion is definitely interesting and postponed, in its quantitative details, to a future research.
For aggregates, the utilization of limit analysis with pre-assigned failure mechanisms can be regarded as a simplified empirical procedure. It bases on the observation of the real damages suffered by masonry buildings with deformable floors during previous earthquakes. The Italian Network of the Earthquake Engineering University Laboratories (ReLUIS) has put at disposal Excel spreadsheets for a semi-automatized estimation of such collapse accelerations [54].

Basing on the aforementioned idea, in the last decades huge developments followed, leading to the introduction of a comprehensive abacus of several possible partial failure mechanisms, with an exhaustive taxonomy of the most common possibilities. The results of the non-linear dynamic analyses here discussed can be regarded as extremely useful, because they give a clear idea of the most vulnerable units and the expected mechanisms. It is therefore possible to restrict the application of limit analysis to a few failure mechanisms, instead of checking all the possibilities in each single unit.

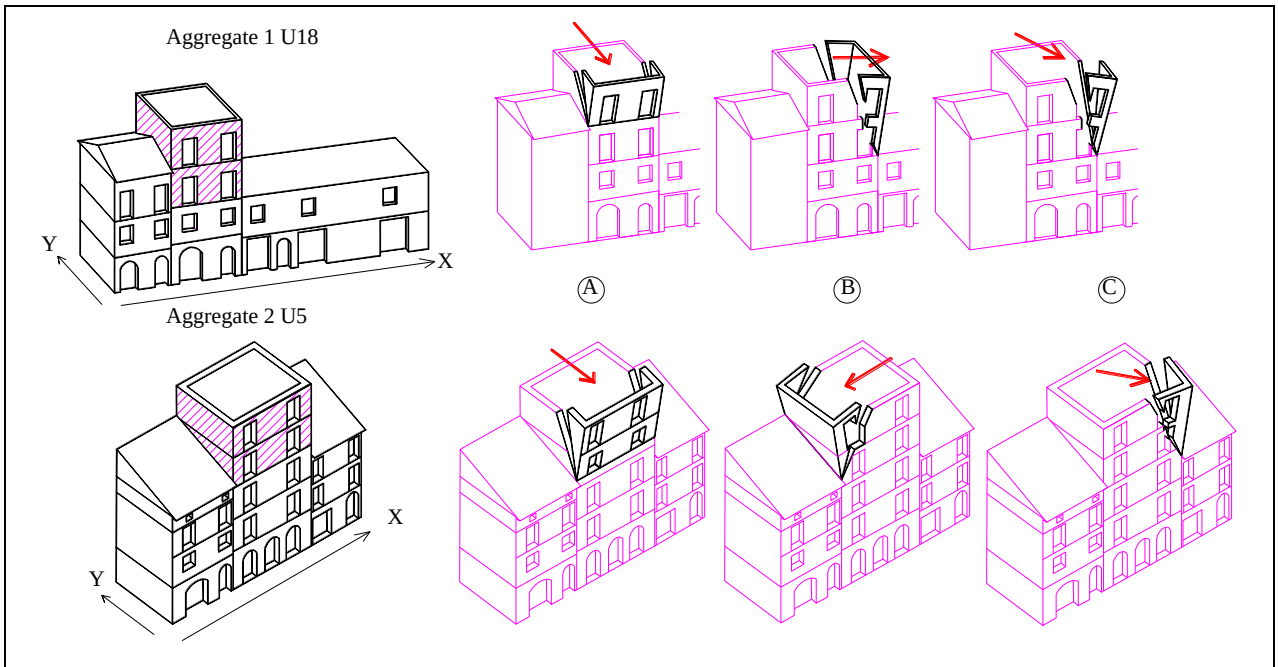

a_g/g	A	B	C
Aggregate 1 - U18	0.12	0.13	0.09
Aggregate 2 - U5	0.13	0.12	0.11

Figure 21. Results of kinematic limit analysis applied on the most vulnerable units. Application of a static horizontal load along the X (A), the Y (B) and contemporarily the X & Y (C) directions. Normalized collapse horizontal accelerations, ag/g, and active failure mechanisms.

As a matter of fact, it is worth mentioning that the role played by the interlocking between perpendicular walls is crucial for the activation of a specific partial out-of-plane failure mechanism, for the determination of its shape as well as for the evaluation of the collapse acceleration. When interlocking is assumed absent, mode 1 failure is a classic overturning mechanism of the wall at the base. The resultant normalized failure acceleration is typically extremely low and dependent exclusively on the geometrical features of the wall, being equal to the ratio between the thickness and the height. In order to consistently compare limit analysis results with non-linear dynamic analyses ones, it is necessary to assume a perfect interlocking in correspondence with the corners. The FE code, indeed, is conceived without any particular adjustment of the corners strength, allowing to account for the effects of a suboptimal interlocking, as for instance the utilization of interface elements with different mechanical characteristics.

As already pointed out, the non-linear dynamic analyses have been performed applying simultaneously the two components of the accelerogram in the longitudinal and transversal directions. The application of accelerograms along two perpendicular directions promotes the activation of out-of-plane partial failure mechanisms with overturning of the most exposed corners (i.e. upper parts of the single units, near the roof, not sufficiently constrained).

The results of the non-linear dynamic analyses show that the most vulnerable units are U18 and U5 for Aggregate 1 and Aggregate 2, respectively. Limit analyses are therefore limited to such units, and

the possible partial failure mechanisms (associated with the minimum multiplier) found are depicted in Figure 21.
Kinematic limit analysis computations show that the corners of the upper stories of units U18 and U5 for Aggregate 1 and Aggregate 2, respectively, are the most vulnerable in the case of the simultaneous application of the seismic action along the X and Y directions. In limit analysis, the independent application of horizontal forces along the geometrical principal axes of the aggregate results - as expected - in an increase of the collapse acceleration: in any case, it is confirmed that U18 and U5 are still the most vulnerable units, with activation of an out-of-plane overturning mechanism of the upper part. The reason is linked to the geometrical features of such units, which result to be either isolated or scarcely connected with neighboring buildings at the upper stories. A similar outcome may be expected performing non-linear dynamic analyses with accelerograms applied separately along the X and Y directions. In non-linear dynamic analyses the PGAs causing the collapse of such portions of the units are finally similar to the ultimate accelerations obtained through the kinematic limit analysis approach previously discussed, confirming that kinematic limit analysis with pre-assigned failure mechanisms can provide preliminary results that are useful for practical purposes.

6. Conclusions

This study has investigated the seismic response of two historical masonry aggregates through non-linear dynamic analyses performed on detailed 3D FE models assuming an elasto-plastic damage constitutive law for masonry. Such a numerical approach is very effective for assessing the seismic response of the whole aggregate, presenting several advantages when compared to the current simplified methods. As a matter of fact, it allows taking into account the dynamic characteristics of the aggregate with reference to the main features of the accelerogram, the torsional effects induced by the seismic action on the perimeter walls located at the extremities of the aggregate, as well as the potential interactions due to the structural contiguity of the units within the aggregate. The non-linear dynamic analyses have highlighted the most vulnerable elements and the damage distribution of the two aggregates for different seismic intensity levels.

The main conclusions that can be drawn from the numerical simulations performed in this study are summarized and shortly discussed below.

- The most relevant modes of both the aggregates present low values of periods: as a result, such structures may experience high amplifications of spectral accelerations and therefore extensive damage. In some cases, the geometrical features are not sufficient to comprehensively explain the seismic behavior and vulnerability of the main walls and critical portions of the aggregates, but also their dynamic properties should be taken into account with reference to the characteristics of the accelerograms considered. The results provided by eigen-frequency analysis associated with the response spectra may preliminarily indicate the critical parts of the aggregate in terms of spectral acceleration amplifications corresponding to the PMR involved. Indeed, as emerged from the present study, eigen-frequency analysis highlights modes characterized by high values of the PMR with vibration periods corresponding to relevant spectral accelerations. Moreover, such modes are particularly influenced by the dynamic behavior of some structural parts of the aggregate that have shown relevant damages at the end of the non-linear dynamic analyses. Such a dynamic behavior is typical of complex structures that are generally characterized by local modes playing a crucial role in the global structural response. In this case, the main findings obtained from modal analysis could be useful to identify the units of the aggregates where a seismic damage concentration is expected. Nevertheless, it is also evident that modal analysis, which is based on a linear-elastic behavior of the model, is not able to account for the influence of the damage

on the dynamic properties of the aggregate and, then, on possible modifications of the cracks distributions among the different structural parts of the aggregate.

- The numerical analyses show the high vulnerability of the perimeter walls that may be prone to overturning mechanisms. In particular, the units at the extremities of the aggregate are subjected to large displacements because they are not efficiently braced by the adjacent units. Moreover, the perimeter walls located at the edges of the aggregate present large displacements due to the torsional effects induced by the seismic action. It is important to point out that the FE model here considered provides damage scenarios influenced by both the in-plane and out-of-plane behavior of walls that interact among them through a continuous 3D model. Although this approach does not explicitly consider rigid-block mechanisms that are at the basis of the kinematic analysis, it allows deriving important information regarding the possible activation of mode 1 failure mechanisms from the results of the non-linear dynamic analyses. Indeed, the distribution and severity of cracks allow identifying both the zones of the aggregate particularly susceptible of damages due to out-of-plane actions and the structural parts where the damage patterns could lead to the subsequent activation of mode 1 failure mechanisms. It is evident that the results obtained from the numerical analyses presented in this paper are influenced by the hypotheses at the basis of the model, including the connections among transversal walls. Such an assumption, which in some cases may not reflect the real status of some parts of the aggregate, has been here introduced in order to gain information on the global response of the aggregate, considering it as a body composed of the effective assemblage of units interacting among them.

- The most damaged elements of each aggregate are generally the walls of the tall units without lateral support and the adjacent slabs covering large spans and characterized by small thickness. The perimeter walls generally exhibit extensive damage in correspondence with the openings and in some cases also at the base, indicating the possible occurrence of overturning mechanisms. The internal walls do not generally exhibit remarkable displacements, except the tall internal walls that are not braced by adjacent units; conversely, they present significant damage, mainly in the connection regions with the diaphragms.

- The structural response of a single unit is affected by the interactions with the adjacent parts due to the structural continuity of the building units composing the aggregate. The perimeter walls exhibit large out-of-plane displacements involving the adjacent walls and the slabs that are largely damaged: such a result is more evident when the walls present several openings and the diaphragms cover large spans. For both the aggregates, the majority of the diaphragms present significant damage at the edges, in the connection regions with the walls, influencing the out-of-plane displacements of the walls.

- The presence of several openings is a fundamental feature that significantly decreases the strength of the perimeter walls, influencing the damage distribution in the aggregate, as it is especially shown by the different crack patterns observed in the east and west sides of Aggregate 2: high EDDTD values are registered for the walls of the west side, which exhibit extensive cracks in correspondence with the numerous openings.

- It can be noted that a good correlation of results in terms of normalized displacements and EDDTD values is found for the critical walls: in both the aggregates, the most damaged walls are generally subjected to large displacements. However, some exceptions can be observed, such as some internal walls, which present extensive damage only in the upper part, and some perimeter walls, which present a damage concentration at the base.

The above outcomes clearly show the importance of the analysis approach here employed to investigate the seismic response of masonry building compounds. Indeed, the use of advanced dynamic analyses based on a non-linear FE model of the whole aggregate allows examining the global response of the system by taking into account the crucial role of the interaction among structural units. The emerged damage scenarios, which can be preliminarily interpreted also on the basis of the results of a modal analysis of the compound, emphasize several vulnerabilities that are particularly influenced by the interaction among the units composing the compound.

References

[1] D'Ayala DF, Paganoni S. Assessment and analysis of damage in L'Aquila historic city centre after 6th April 2009. Bulletin of Earthquake Engineering 2011;9(1):81-104.

[2] Penna A, Morandi P, Rota M, Manzini CF, Da Porto F, Magenes G. Performance of masonry buildings during the Emilia 2012 earthquake. Bulletin of Earthquake Engineering 2014;12(5):2255-2273.

[3] Carocci CF. Small centres damaged by 2009 L'Aquila earthquake: on site analyses of historical masonry aggregates. Bulletin of Earthquake Engineering 2012;10(1):45-71.

[4] Vona M, Cascini G, Mastroberti M, Murgante B, Nolè G. Characterization of URM buildings and evaluation of damages in a historical center for the seismic risk mitigation and emergency management. International Journal of Disaster Risk Reduction 2017;24:251-263.

[5] Clementi F, Gazzani V, Poiani M, Lenci, S. Assessment of seismic behaviour of heritage masonry buildings using numerical modelling. Journal of Building Engineering 2016;8:29-47.

[6] Fagundes C, Bento R, Cattari S. On the seismic response of buildings in aggregate: Analysis of a typical masonry building from Azores. Structures 2017;10:184-196.

[7] Ferrito T, Milosevic J, Bento R. Seismic vulnerability assessment of a mixed masonry-RC building aggregate by linear and nonlinear analyses. Bulletin of Earthquake Engineering 2016;14(8):2299-2327.

[8] Neves N, Arêde A, Costa A. Seismic analysis of a building block. Bulletin of Earthquake Engineering 2012;10(1):235-267.

[9] Pujades LG, Barbat AH, González-Drigo R, Avila J, Lagomarsino S. Seismic performance of a block of buildings representative of the typical construction in the Eixample district in Barcelona (Spain). Bulletin of Earthquake Engineering 2012;10(1):331-349.

[10] Ulrich T, Negulescu C, Ducellier A. Using the discrete element method to assess the seismic vulnerability of aggregated masonry buildings. Bulletin of Earthquake Engineering 2015;13(10):3135-3150.

[11] DM 17/01/2018. Aggiornamento delle "Norme tecniche per le costruzioni". Ministero delle Infrastrutture e Trasporti (GU n.42 20/02/2008), Rome, Italy. [Update of the "Technical norms on constructions].

[12] Circolare n° 617 del 2 febbraio 2009. Istruzioni per l'applicazione delle nuove norme tecniche per le costruzioni di cui al decreto ministeriale 14 gennaio 2008. [Instructions for the application of the new technical norms on constructions].

[13] DPCM 9/2/2011. Linee guida per la valutazione e la riduzione del rischio sismico del patrimonio culturale con riferimento alle Norme tecniche delle costruzioni di cui al decreto del Ministero delle Infrastrutture e dei trasporti del 14 gennaio 2008. [Italian guidelines for the evaluation and the reduction of the seismic risk for the built heritage, with reference to the Italian norm of constructions].

[14] Formisano A, Florio G, Landolfo R, Mazzolani FM. Numerical calibration of an easy method for seismic behaviour assessment on large scale of masonry building aggregates. Advances in Engineering Software 2015;80:116-138.

[15] Maio R, Vicente R, Formisano A, Varum H. Seismic vulnerability of building aggregates through hybrid and indirect assessment techniques. Bulletin of Earthquake Engineering 2015;13(10):2995-3014.

[16] Formisano A. Theoretical and numerical seismic analysis of masonry building aggregates: case studies in San Pio Delle Camere (L'Aquila, Italy). Journal of Earthquake Engineering 2017;21(2):227-245.

[17] Formisano A. Local-and global-scale seismic analyses of historical masonry compounds in San Pio delle Camere (L'Aquila, Italy). Natural Hazards 2017;86(2):465-487.

[18] Formisano A., Massimilla A. A novel procedure for simplified nonlinear numerical modeling of structural units in masonry aggregates. International Journal of Architectural Heritage 2018, https://doi.org/10.1080/15583058.2018.1503365

[19] Cardoso R, Lopes M, Bento R. Seismic evaluation of old masonry buildings. Part I: Method description and application to a case-study. Engineering Structures 2005; 27(14): 2024-2035.

[20] Ramos LF, Lourenço PB. Modeling and vulnerability of historical city centers in seismic areas: A case study in Lisbon. Engineering Structures 2004; 26(9): 1295-1310.

[21] Giamundo V, Sarhosis V, Lignola GP, Sheng Y, Manfredi G. Evaluation of different computational modelling strategies for the analysis of low strength masonry structures. Engineering Structures 2014; 73: 160-169.

[22] Cascini L, Portioli F, Landolfo R. 3D rigid block micro-modelling of a full-scale unreinforced brick masonry building using mathematical programming. International Journal of Masonry Research and Innovation 2016; 1(3): 189-206.

[23] Sarhosis V, Dais D, Smyrou E, Bal IE. Evaluation of modelling strategies for estimating cumulative damage on Groningen masonry buildings due to recursive induced earthquakes. Bulletin of Earthquake Engineering 2019; In press.

[24] Nikolic Ž, Smoljanovic H, Živaljic N. Numerical analysis of masonry structures by finite-discrete element model. International Journal of Masonry Research and Innovation 2016; 1(4): 330-350.

[25] Forgács T, Sarhosis V, Bagi K. Minimum thickness of semi-circular skewed masonry arches. Engineering Structures 2017; 140: 317-336.

[26] Drei A., Milani G, Sincraian G. DEM numerical approach for masonry aqueducts in seismic zone: two valuable Portuguese examples. International Journal of Masonry Research and Innovation 2017; 2(1): 1-29.

[27] Lemos JV. Contact representation in rigid block models of masonry. International Journal of Masonry Research and Innovation 2017; 2(4): 321-334.

[28] Chiozzi A, Milani G, Grillanda N, Tralli A. A fast and general upper-bound limit analysis approach for out-of-plane loaded masonry walls. Meccanica 2018; 53: 1875-1898.

[29] Chiozzi A, Grillanda N, Milani G, Tralli A. UB-ALMANAC: an adaptive limit analysis NURBS-based program for the automatic assessment of partial failure mechanisms in masonry churches. Engineering Failure Analysis 2018; 85: 201-220.

[30] Milani G, Shehu R, Valente M. Possibilities and limitations of innovative retrofitting for masonry churches: Advanced computations on three case studies. Construction and Building Materials 2017:147;239-263.

[31] Milani G, Shehu R, Valente M. A kinematic limit analysis approach for seismic retrofitting of masonry towers through steel tie-rods. Engineering Structures 2018;160:212-228.

[32] Barbieri G, Valente M, Biolzi L, Togliani C, Fregonese L, Stanga G. An insight in the late Baroque architecture: an integrated approach for a unique Bibiena church. Journal of Cultural Heritage 2017;23:58-67.

[33] Valente M, Milani G. Damage survey, simplified assessment, and advanced seismic analyses of two masonry churches after the 2012 Emilia earthquake. International Journal of Architectural Heritage 2018. https://doi.org/10.1080/15583058.2018.1492646.

[34] Betti M, Bartoli G, Orlando M. Evaluation study on structural fault of a Renaissance Italian palace. Engineering Structures 2010;32(7):1801-1813.

[35] Sandoval C, Valledor R, Lopez-Garcia D. Numerical assessment of accumulated seismic damage in a historic masonry building. A case study. International Journal of Architectural Heritage 2017;11(8):1177-1194

[36] Formisano A, Grande E, Valente M, Milani G (2019). Simplified approaches for the seismic assessment of complex masonry building aggregates: Validation against full 3D FE non-linear dynamic simulations on a case study in Italy. Under review.

[37] Saccucci M. Il rilievo degli edifici storici nella CLE: simulazione dei possibili cinematismi di collasso. Degree Thesis – University of Cassino and Southern Lazio –Italy 2016.

[38] Pelliccio A, Saccucci M, Grande E. HT_BIM: Parametric modelling for the assessment of risk in historic centers 7HT_BIM: La modellazione parametrica per l'analisi del rischio nei centri storici. Disegnare con 2017;10(18).

[39] ABAQUS®, Theory Manual, Version 6.14.

[40] Lubliner J, Oliver J, Oller S, Oñate E. A plastic-damage model for concrete. International Journal of Solids and Structures 1989;25:299-326.

[41] Lee J., Fenves G.L. Plastic-Damage Model for Cyclic Loading of Concrete Structures (1998). Journal of Engineering Mechanics 124, 892-900.

[42] Valente M, Milani G. Effects of geometrical features on the seismic response of historical masonry towers. Journal of Earthquake Engineering 2018, Supp. 1, 2-34.

[43] Ubertini F, Cavalagli N, Kita A, Comanducci G. Assessment of a monumental masonry bell-tower after 2016 Central Italy seismic sequence by long-term SHM. Bulletin of Earthquake Engineering 2018;16(2):775-801.

[44] Valente M, Milani G. Damage assessment and collapse investigation of three historical masonry palaces under seismic actions. Engineering Failure Analysis 2019, 98, 10-37.

[45] Valente M, Barbieri G, Biolzi L. Seismic assessment of two masonry Baroque churches damaged by the 2012 Emilia earthquake. Engineering Failure Analysis 2017;79:773-802.

[46] Valente M, Milani G. Damage assessment and partial failure mechanisms activation of historical masonry churches under seismic actions: Three case studies in Mantua. Engineering Failure Analysis 2018;92:495-519.

[47] Valente M, Milani G. Seismic response and damage patterns of masonry churches: seven case studies in Ferrara, Italy. Engineering Structures 2018, 177.

[48] Castellazzi G, D'Altri AM, de Miranda S, Ubertini F. An innovative numerical modeling strategy for the structural analysis of historical monumental buildings. Engineering Structures 2017;132:229-248.

[49] Van der Plujm R. Material properties and its components under tension and shear. In Proc. 6th Canadian Masonry Symposium 1992.

[50] Page A. The biaxial compressive strength of brick masonry. Proceedings of the Institution of Civil Engineers 1981.

[51] Milani G, Lourenço PB, Tralli A. Homogenised limit analysis of masonry walls, Part I: Failure surfaces. Computers & Structures 2006: 84 (3-4): 166-180.

[52] Brandonisio G, Lucibello G, Mele E, De Luca A. Damage and performance evaluation of masonry churches in the 2009 L'Aquila earthquake. Engineering Failure Analysis 2013; 34: 693-714.

[53] Kita A, Cavalagli N, Ubertini F. Temperature effects on static and dynamic behavior of Consoli Palace in Gubbio, Italy. Mechanical Systems and Signal Processing 2019; 120: 180-202.

[54] Milano L, Mannella A, Morisi C, Martinelli A. Schede illustrative dei principali meccanismi di collasso locali negli edifici esistenti in muratura e dei relativi modelli cinematici di analisi. ReLUIS report of the "Network of the Italian Universities Laboratories of Earthquake Engineering" 2010. www.reluis.it